CRN 96-38

Microscopic Study of Superdeformed Rotational Bands in ^{151}Tb

N. El Aouad, J. Dobaczewski, J. Dudek, X. Li, W.D. Luo
H. Molique, A. Bouguettoucha, Th. Byrski, F. Beck
C. Finck and B. Kharraja

CENTRE DE RECHERCHES NUCLEAIRES

STRASBOURG

IN2P3 CNRS

UNIVERSITE LOUIS PASTEUR

Microscopic Study of Superdeformed Rotational Bands in ^{151}Tb

N. El Aouad, J.Dobaczewski,* J. Dudek, X. Li, W.D. Luo, H. Molique, A. Bouguettoucha, Th. Byrski, F. Beck, and C. Finck

Centre de Recherches Nucléaires, IN_2P_3-CNRS/Université Louis Pasteur, F-67037 Strasbourg Cedex 2, France

B. Kharraja

Centre de Recherches Nucléaires, IN_2P_3-CNRS/Université Louis Pasteur, F-67037 Strasbourg Cedex 2, France

Department of Physics, University Chouaib Doukkali, BP20 El-Jadida, Marocco

University of Notre Dame, Department of Physics, Notre Dame, IN 46556, USA

Abstract

Structure of eight superdeformed bands in the nucleus ^{151}Tb is analyzed using the results of the Hartree-Fock and Woods-Saxon cranking approaches. It is demonstrated that far going similarities between the two approaches exist and predictions related to the structure of rotational bands calculated within the two models are nearly parallel. An interpretation scenario for the structure of the superdeformed bands is presented and predictions related to the exit spins are made. Small but systematic discrepancies between experiment and theory, analyzed in terms of the dynamical moments, $\mathcal{J}^{(2)}$, are shown to exist. The pairing correlations taken into account by using the particle-number-projection technique are shown to *increase* the disagreement. Sources of these systematic discrepancies are discussed – they are most likely related to the yet not optimal parametrization of the nuclear interactions used.

PACS number(s): 21.60.Ev, 21.10.Re, 21.60.Jz, 27.70.+q

Typeset using REVTEX

*Permanent address: Institute of Theoretical Physics, Warsaw University, Hoża 69, PL-00681 Warsaw, Poland

I. INTRODUCTION

In the present article the results of microscopic calculations for the high spin properties of the superdeformed (SD) rotational bands in the nucleus ^{151}Tb are presented. This nucleus is a direct neighbor of the "doubly magic" superdeformed nucleus ^{152}Dy which is characterized by particularly large gaps in the neutron and proton deformed single-particle spectra. We investigate the rotational bands together with their microscopic structure in terms of the single-particle orbitals.

The theoretical description of such properties, most often applied in the literature, is based on the average field approximation (see Ref. [1] for a recent review). Most of the present knowledge about the nucleonic structure underlying the properties of the SD rotational bands comes from analyzing the single-particle Routhians generated by making use of the rotating Nilsson or deformed Woods-Saxon (WS) Hamiltonians. The total nuclear energy as a function of spin is then obtained by using the Strutinsky total energy expression (see for example Ref. [2] and references therein). Similar analyses based on the Hartree-Fock (HF) [3–9], or relativistic mean field (RMF) [10–12] approximations are more difficult and have not been, up to now, applied for global calculations, with the notable exception of Ref. [12]. However, they have an advantage of directly providing the total energy as a function of spin which can be compared with the experimental data. In the present work we apply and compare the WS and HF cranking approximations.

Uncertainties in predictions coming from various models lead to ambiguities in the interpretation of the experimental results. The problem of a (non-)uniqueness in the interpretation of the microscopic structure of SD bands is strongly aggravated by the fact that the spins of nearly all measured bands in question are not known. Moreover, the nuclear interactions responsible for the single-particle level ordering in the strongly deformed nuclei are obtained mainly by extrapolating the properties of the interactions known from spherical and moderately deformed nuclei.

Direct tests of the structure of wave functions of the single-nucleonic orbitals (via e.g. magnetic moments) are considered extremely difficult from the experimental point of view due to the very short life-times of the SD high-spin states. In such a situation we are confronted not only with the problem of a microscopic interpretation of the quickly growing body of the experimental information — but also with the problem of a cross-check analysis of theoretical predictions coming from distinct nuclear interactions used. It will be one of our objectives to provide such a test by comparing the microscopic properties calculated within the Strutinsky and HF methods.

For a realization of our objective, the experimental knowledge of eight bands in one single SD nucleus, ^{151}Tb, is extremely useful. At present there are only very few nuclei in which the number of known SD bands is comparable to that in ^{151}Tb. Moreover, the transition energies of those bands behave regularly as functions of the angular momentum I. Such a regularity provides the optimal conditions for theoretical verifications of single-nucleonic configurations via the dynamical moments defined by

$$\mathcal{J}^{(2)} = \frac{dI}{d\omega}. \tag{1.1}$$

This is so, because the abrupt band crossings (relatively abundant in other nuclei) may otherwise cause strong variations of $\mathcal{J}^{(2)}$-moments as a function of ω, thus rendering the

comparisons of the typical behavior (and values) of the $\mathcal{J}^{(2)}$-moments with experiment less direct. In some cases the band crossings may play an important role in helping to identify some orbitals via the characteristic crossing frequencies. However, we found it preferable to first discuss the structural elements, such as the global behavior of the $\mathcal{J}^{(2)}$-moments and their values, in relation with some characteristic nucleonic configurations. Another group of problems related to the band crossings, crossing frequency systematics and alignments is left for future investigations.

An advantage of basing the verification of the theoretical results with experiment on the $\mathcal{J}^{(2)}$-moments is that this quantity does not depend on the exit spin (the spin corresponding to the lowest observed transition in an SD band) while many other quantities do. For this reason we intend to focus on the rotational frequency rather than spin as an independent variable in function of which several microscopically calculated quantities will be displayed. However, the question of the relative spins in the multi-band problem, or equivalently, of the relations between the exit spins in the bands observed, is one of the most urgent at present. For this reason a special section will be devoted to discussing the total energy vs. spin dependence, $\mathcal{E} = \mathcal{E}(I)$.

Let us mention here that, similarly to numerous other studies devoted to the interpretation of the intrinsic configurations of the SD bands, our work will not be able to give definite answers in several points. We feel, nevertheless, that our method allows to pin down relatively reliably at least the possible alternative interpretations of the bands in question.

While the lack of knowledge of the exit spins remains one of the most serious experimental problem, many analyses of the SD nuclei have benefited from the strong similarities between various bands in various SD nuclei (the "identical band" correlations, cf. Ref. [13] for a recent review). By comparing the theoretically predicted structures of the bands related by the "identicality" (or "sameness") relations, it was possible to confirm or eliminate certain hypotheses related to the underlying single-nucleonic structure. This type of correlations are abundant in the ^{151}Tb nucleus and will be used to further test the microscopic results and predictions.

It is expected that some amount of pairing correlations remains in the SD bands up to the highest spins measured and that the pairing correlations decrease with increasing angular momentum. Although, as we will demonstrate it, in the ^{151}Tb nucleus the most important properties of the SD bands such as, e.g., the behavior of the dynamical moments in function of the rotational frequency can be described reasonably well without taking into account the pairing, the systematic small discrepancies which exist, are increasing when the pairing correlations are taken into account. Moreover, the arguments will be given demonstrating that at least in the case of some parametrizations of the nuclear interactions another source of small systematic deviations between theory and experiment may be attributed to slightly exaggerated nuclear volumes as calculated within the mean field approaches (cf. Sec. V for details).

A number of structural features related to the high-spin behavior of the SD nuclei in the A$\sim$150 region have been discussed in the literature. Early studies were based on the Nilsson or WS cranking approaches, and performed without pairing [14] or with the dynamic pairing correlation [15–18] taken into account by using either the random phase approximation (RPA) or the particle number projection (PNP) together with the monopole pairing interaction. In most of those early studies the experimental information has been strongly

limited, as compared to the amount of data available today. In more recent studies, the WS [19] or the Hartree-Fock-Bogolyubov (HFB) [9] methods have been applied to a few low-lying bands in a number of selected A$\sim$150 nuclei with pairing correlations treated in terms of the Lipkin-Nogami method.

The present study differs from the previously published ones in the following: (i) due to a rich experimental information available now, we can concentrate on systematic discrepancies between the theoretical and experimental data, (ii) we discuss the analogies and differences between the self-consistent (HF) and the non-self-consistent (WS) cranking approaches within the same analysis (applied simultaneously on a common set of experimental data), (iii) we analyze simultaneously all available data in the nucleus in question, (iv) by applying the particle-number-projected pairing approach we are able to show that the systematic discrepancies cannot be attributed to the pairing correlations, and consequently (v) we arrive at a suggestion that a modification of the underlying interactions will be needed in order to improve the agreement with data.

II. SUMMARY OF THE EXPERIMENTAL RESULTS

As mentioned earlier, in the ^{151}Tb nucleus eight SD bands have been observed. In addition to the two SD bands discovered relatively early [20,21], six new SD bands have been found and assigned to this nucleus recently [22,23] using the EUROGAM spectrometer. Those recent data were obtained from experiments at the Nuclear Structure Facility, Daresbury Laboratory, using the ^{130}Te(^{27}Al,6n)^{151}Tb reaction at a bombarding energy of 154 MeV. The details of the experimental procedure can be found in [22,23]; here we only recall that the γ-rays were detected by the EUROGAM spectrometer [24,25] which consisted, for this experiment, of 42 operational Ge detectors. The data rates in the individual Ge detectors were 7-9 kHz. The trigger condition used to select unsuppressed events was that at least 7 Ge detectors were involved in a coincidence. After the suppression requirement was included, the average number of coincident detectors dropped to $\sim$3.9. A total data set of 5.5×10^8 suppressed events with Ge fold $\geq$ 3 was recorded and after unpacking the high-fold-multiplicity events led to 3.1 $\times10^9$ γ^4 coincidences. The final spectra were obtained by summing combinations of 3-dimensional gates set on the SD transitions in a 4-dimensional analysis [24].

The assignment of the new 6 excited SD bands to ^{151}Tb was based on an unambiguous evidence of known γ-ray transitions of the normal deformed nucleus following the de-excitation from the SD band members. The SD bands have been labeled 1,2,3,...,8. The previously reported SD bands have been labeled 1 (called the yrast band, although its position in energy with respect to other bands is not experimentally established) and 2 (the band which shows a remarkable similarity in terms of the γ-ray energies with the SD Band 1 of ^{152}Dy). The other excited SD bands have been arbitrarily attributed labels ranging from 3 to 8.

Employing the same reaction, the ^{151}Tb nucleus has been recently reinvestigated using the Eurogam II array installed at the Vivitron accelerator of the *Centre de Recherches Nucléaires* in Strasbourg. This array consisted of 54 high-efficiency Ge detectors (30 tapered coaxial detectors and 24 clover detectors) providing a photopeak efficiency of 7.4% at 1.33 MeV. With the large statistics and high peak-to-background ratio, it has been possible to obtain a higher precision of the SD γ-ray transition energies which in the present study are

used to extract accurate values of the corresponding dynamic moments. The experimental results for Bands 1 and 2 are presented in Table I.

The intensities (with uncertainties) of the different bands relative to the yrast band are: 50(5)% (Band 2), 35(5)% (Band 3), 6(2)% (Band 4), 10(2)% (Band 5), 9(2)% (Band 6), 11(2)% (Band 7), 7(3)% (Band 8).

Let us also mention that in the determination of the experimental frequencies and dynamic moments we use the expressions

$$\begin{aligned}\hbar\omega(I) &= \frac{E(I+2)-E(I-2)}{4} \\ &= \frac{E_\gamma(I+2)+E_\gamma(I)}{4}\end{aligned} \tag{2.1a}$$

$$\begin{aligned}\mathcal{J}^{(2)}(I) &= \frac{4\hbar^2}{E(I+2)-2E(I)+E(I-2)} \\ &= \frac{4\hbar^2}{E_\gamma(I+2)-E_\gamma(I)}\end{aligned} \tag{2.1b}$$

where $E_\gamma(I)=E(I)-E(I-2)$.

III. WOODS-SAXON CALCULATIONS

In this Section we summarize the main points of the calculations based on the average nuclear field with the deformed WS potential. The following three subsections present: (i) the structure of the Hamiltonian used, Sec. III A, (ii) some remarks related to the self-consistency in the case of *a priori* non-self-consistent formalism with the WS potential, Sec. III B, and (iii) a short description of the actual variant of the Strutinsky method applied, Sec. III C. The details can be found in the literature cited below and will not be repeated here. Even though most of the mathematical expressions are available in the literature, there exist differences in notation between various authors, and we found important to recall the definitions of some basic quantities.

A. Deformed Woods-Saxon Hamiltonian and the cranking approximation

The single-nucleonic energies and wave functions for nucleons moving in the deformed potential of the WS type,

$$V(\boldsymbol{r};V_0,\kappa,a,r_0)=\frac{V_0[1\pm\kappa\frac{N-Z}{N+Z}]}{\{1+\exp[\mathrm{dist}_{\Sigma_0}(\boldsymbol{r};r_0)/a]\}}, \tag{3.1}$$

are found by solving the corresponding Schrödinger equation. The spin-orbit term is included in the usual deformation-dependent form:

$$\begin{aligned}\hat{V}_{\mathrm{SO}}(\boldsymbol{r},\boldsymbol{p};V_0^{\mathrm{SO}},\kappa,a_{\mathrm{SO}},r_{\mathrm{SO}}) &= \lambda\left(\frac{\hbar}{2mc}\right)^2 \\ &\times\left\{\left[\boldsymbol{\nabla}\frac{V_0[1\pm\kappa\frac{N-Z}{N+Z}]}{\{1+\exp[\mathrm{dist}_{\Sigma_{\mathrm{SO}}}(\boldsymbol{r};r_{\mathrm{SO}})/a_{\mathrm{SO}}]\}}\right]\times\boldsymbol{p}\right\}\cdot\boldsymbol{s},\end{aligned} \tag{3.2}$$

and the Coulomb potential is added for protons. In the above relations the "+" sign applies for protons and the "−" sign for neutrons, while $\boldsymbol{p}$ and $\boldsymbol{s}$ denote the linear momentum and the spin operators, respectively. For reasons of compatibility with previous studies, we keep the factor $[\hbar/(2mc)]^2$ in the definition of the spin-orbit potential (m is the nucleonic mass). Then the spin-orbit strength parameter, λ, is a dimensionless quantity. We use $\lambda = 35$ for neutrons and $\lambda = 36$ for protons.

The nuclear surfaces Σ_0 and Σ_{SO}, defining the central and spin-orbit fields, respectively, are expressed in terms of the spherical harmonics as

$$\Sigma_{0(SO)}: \; R(\theta,\phi) = R_{0(SO)}c(\alpha)\left[1 + \sum_{\lambda=0}^{\lambda_{max}} \alpha_{\lambda\mu}Y_{\lambda\mu}(\theta,\phi)\right]. \tag{3.3}$$

In the above relation, $c(\alpha)$ is a function of all the deformation parameters that guarantees the constant volume for any deformation, and $R_{0(SO)} = r_{0(SO)}A^{1/3}$ with the central-potential radius parameter $r_0 = 1.347\,\mathrm{fm}$ for neutrons and $r_0 = 1.275\,\mathrm{fm}$ for protons; similarly $r_{SO} = 1.310\,\mathrm{fm}$ for neutrons and $r_{SO} = 1.200\,\mathrm{fm}$ for protons. The central-potential depth-parameters are: $V_0 = -49.6\,\mathrm{MeV}$ and $\kappa = 0.86$ while the diffuseness parameters are $a = 0.70\,\mathrm{fm}$ for the central part and $a_{SO} = 0.70\,\mathrm{fm}$ for the spin-obit part of the potential, independently of the isospin (for details see Refs. [26] and [27]). Finally, the geometrical distance of a point $\boldsymbol{r}$ from the auxiliary surfaces $\Sigma_{0(SO)}$ defined above is denoted by $\mathrm{dist}_{\Sigma_{0(SO)}}$; the latter quantity is negative for $\boldsymbol{r}$ in the nuclear interior and positive otherwise.

In our calculations we allow for the total Routhian (for definition of the Routhians see the following sections) minimization with the deformation-mesh defined by

$$\alpha_{20} = 0.400, 0.425, \ldots, 0.800 \text{ (17 points)} \tag{3.4}$$

and

$$\alpha_{40} = 0.020, 0.040, \ldots, 0.180 \text{ (9 points)} \tag{3.5}$$

with α_{22} corresponding to 5 "planes" for fixed γ deformations [$\alpha_{20} = \beta\cos(\gamma)$ and $\alpha_{22} = \frac{1}{\sqrt{2}}\beta\sin(\gamma)$] as follows

$$\gamma = -10°, 5°, \ldots, 10° \text{ (5 points)}. \tag{3.6}$$

We solve the cranking equations of the standard form

$$\hat{h}^{\omega}\psi_n^{\omega} = e_n^{\omega}\psi_n^{\omega} \tag{3.7}$$

for

$$\hbar\omega = 0.00, 0.05, \ldots, 1.50\,MeV \text{ (31 points)} \tag{3.8}$$

with

$$\hat{h}^{\omega} = \hat{T} + V + \hat{V}_{SO} + V_C - \omega\hat{I}_y, \tag{3.9}$$

where the WS potential V and the related spin-orbit term $\hat{V}_{SO}$ are defined in Eqs. (3.1) and (3.2) while the Coulomb potential V_C is that of the classical uniform sharp-edge charge distribution corresponding to the actual nuclear shape.

As always in numerical calculations of the matrix elements used for constructing the Hamiltonian matrix, both the number of basis states and the number of points in the Gauss-Hermite integration formulae have been selected in such a way that the final results do not depend in any significant way of that choice (for more details see Ref. [2]). In our case the number of the deformed harmonic-oscillator states used in each of the two parities was about 300.

B. Self-consistency between the potential and density

In the following, the results of the cranking calculations performed within the HF approach will be compared with those obtained for the deformed WS potential. Although it is not possible to formulate the self-consistency concept in the two approaches in the same way, and the WS calculations are *a priori* considered non-self-consistent, it will be of some importance to recall that our way of defining the deformed WS potential imposes a correlation between the equipotential surfaces

$$V(\boldsymbol{r}) = \text{const.}, \tag{3.10}$$

and the surfaces of the constant density defined by

$$\rho(\boldsymbol{r}) = \sum_n \psi_n^*(\boldsymbol{r})\psi_n(\boldsymbol{r}) = \text{const.}, \tag{3.11}$$

as discussed in detail in [28]. The second-order Thomas-Fermi expression [29] for the density functional reads

$$\begin{aligned}\rho(\boldsymbol{r}) = \frac{1}{3\pi^2}\left[\frac{2m}{\hbar^2}(\lambda - V(\boldsymbol{r}))\right]^{3/2} \\ \times\left\{1 - \frac{1}{8}\frac{\hbar^2}{2m}\left[\frac{\boldsymbol{\nabla}V(\boldsymbol{r})\cdot\boldsymbol{\nabla}V(\boldsymbol{r})}{4[\lambda - V(\boldsymbol{r})]^3}\right] + \frac{\Delta V(\boldsymbol{r})}{[\lambda - V(\boldsymbol{r})]^2}\right\},\end{aligned} \tag{3.12}$$

where the terms of the order $\mathcal{O}(\hbar^4)$ have been neglected. Requiring that the potential is equal to a constant, cf. Eq. (3.10), implies by virtue of Eq. (3.1) that

$$\text{dist}(\boldsymbol{r}) = \text{const.}, \tag{3.13}$$

Using the fact that

$$\boldsymbol{\nabla}\text{dist}(\boldsymbol{r})\cdot\boldsymbol{\nabla}\text{dist}(\boldsymbol{r}) = 1, \tag{3.14}$$

and that

$$\Delta\text{dist}(\boldsymbol{r}) = \text{const.} \tag{3.15}$$

for $\boldsymbol{r}$ belonging to the equipotential surface, one obtains after elementary transformations, cf. Ref. [28], that also

$$\boldsymbol{\nabla}V(\boldsymbol{r})\cdot\boldsymbol{\nabla}V(\boldsymbol{r}) = \text{const.} \quad \text{and} \quad \Delta V(\boldsymbol{r}) = \text{const.} \tag{3.16}$$

As a result, at least within the accuracy of $\mathcal{O}(\hbar^4)$ in the Thomas-Fermi approximation, condition (3.10) implies condition (3.11). Such a correlation between the geometry of the potential and that of the density is not valid generally. Neither the Nilsson model nor a deformed WS potential with another type of argument in the exponent of Eq. (3.1), as used sometimes by other authors, gives such a correlation.

Obviously, the spin-orbit term may modify the above result (cf. e.g. Ref. [30]), but since this term has, on the average, matrix elements which are nearly an order of magnitude weaker as compared to those of the central part, its effect in the discussed context is also expected to be relatively weak.

Anticipating some of our results presented below, and in particular surprising similarities between the high-spin behavior properties obtained by using the self-consistent HF method and a non-self-consistent approach with the deformed WS Hamiltonian, one should bear in mind the particular property of definition (3.1) used in this study.

C. Strutinsky method and the total-Routhian calculations

There are numerous presentations of the Strutinsky method, as given for example in the original articles [31,32], and then applied to finite potentials (as e.g. in Ref. [33]). Here we closely follow the presentation given in Ref. [2], and we only briefly discuss the total-Routhian-surface calculations, for which several authors use prescriptions slightly differing in details.

Our calculations of the total nuclear Routhians are based on the expression

$$R^{\omega} = E^{\omega=0}_{\rm macro} + E^{\omega=0}_{\rm micro} + \sum_n (e^{\omega}_n - e^{\omega=0}_n), \tag{3.17}$$

where the summation extends over all the occupied nucleonic states (i.e., in particular takes into account the particle-hole excitations with respect to the reference configuration introduced in Sec. V). The microscopic (or shell) energy is defined as usual by

$$E^{\omega=0}_{\rm micro} = \sum e^{\omega=0}_{\nu} - < \sum e^{\omega=0}_{\nu} >_{\rm shell} \tag{3.18}$$

where the summation over ν extends now over all the single-nucleonic states of the reference configuration. The last term denotes the results of the Strutinsky averaging procedure. This averaging depends on two standard parameters: the smoothing-polynomial order p and the averaging width $\gamma_{\rm av}$. In our applications we have $p = 6$ and $\gamma_{\rm av} = 3.2\,\hbar\omega_{\rm shell}$ with $\hbar\omega_{\rm shell} = 41/A^{1/3}$ MeV. Arguments related to the stability of the final result with respect to (small) uncertainties in these parameters can be found in several publications, see e.g. Ref. [2] and references therein.

IV. HARTREE-FOCK CALCULATIONS

In the following Sections, some details of a particular realization of the HF approach in our study will be described; most of the formal development can be found in the literature and are also summarized in Ref. [34]. Section IV A presents some technical aspects related to the harmonic oscillator basis employed, the numerical calculations of the $\mathcal{J}^{(2)}$-moments

are discussed in Sec. IV B, and the use of the quadrupole constraint to stabilize the iteration process is briefly commented in Sec. IV C.

A. Harmonic-oscillator basis

In the present study we have performed the HF calculations of SD rotational bands using the Skyrme effective interaction. For this purpose a new numerical code HFODD has been constructed [34] which uses the three-dimensional Cartesian deformed harmonic oscillator (HO) basis. The HO basis has up to now been used in solving the HF equations with the Gogny interaction [35–39]. On the other hand, for the Skyrme interaction this method has been used at early stages of investigations [40] and then abandoned in favor of the calculations in spatial coordinates [3,4].

The main advantage of using the spatial coordinates consists in the fact that one may use the same spatial grid of points to treat nuclei of different deformations, while in the former method the basis parameters may need to be adjusted with varying deformation. (The sensitivity of the results with respect to this kind of a dependence decreases with an increasing harmonic-oscillator basis cut-off; in principle the problem disappears in the limit of an infinite basis). However, the SD states have very similar deformations in many neighboring nuclei, and in such a case this particular deficiency disappears. We may then profit from the fact that the calculations which use the HO basis are in general much more stable, have better convergence properties, and hence require less computational effort.

The details concerning the HFODD code will be presented elsewhere [34]; here we only give a few of its basic characteristics pertaining to the present application. The calculations have been performed using a fixed basis given by the HO frequencies $\hbar\omega_\perp$=11.200 MeV and $\hbar\omega_\parallel$=6.246 MeV in the directions perpendicular and parallel to the harmonic-oscillator symmetry-axis, respectively. These values have been obtained by standard prescriptions developed for diagonalizing the deformed WS Hamiltonian [26] in the HO basis, and correspond to the WS potential with the deformations β_2=0.61 and β_4=0.10. The basis has been restricted to the fixed number M of HO states, i.e., keeping the lowest M single-particle energies $\epsilon_{HO}=(n_x+n_y+1)\hbar\omega_\perp + (n_z+\frac{1}{2})\hbar\omega_\parallel$. The actual calculations have been performed with M=306. This corresponds to the maximal numbers of oscillator quanta equal to 8 and 15 in the perpendicular and parallel directions, respectively.

The stability of results with respect to increasing the size of the HO basis is the main concern in all analyses using this technique, and have been studied in detail in Ref. [34]. In fact it is well known that the total energies are very slowly convergent as functions of the basis size. Indeed, in the present calculations a similar effect is seen when we increase the basis from M=306 to M=604, which corresponds to reaching the maximal numbers of 11 and 20 HO quanta in the two main directions. Then the total energy of the yrast configuration of ^{151}Tb at the rotational frequency of $\hbar\omega$=0.6 MeV decreases from −1199.322 to −1201.889 MeV. A similar mechanism is well known also from other type of studies, with the Schrödinger equation diagonalized in a given basis (as for instance with the WS or the folded Yukawa-type potentials). Fortunately the relative (excitation) energies become stable for smaller bases than the absolute values [34].

None of the interesting rotational properties depends in a significant way on an increase of the basis from M=306 to M=604. For example, we obtain the changes of the average

angular momentum from 59.95 to 59.99 $\hbar$, of the mass quadrupole moment from 39.82 to 39.90 b, and of the mass hexadecapole moment [41] from 4.21 to 4.24 b^2. The relative changes as function of $\hbar\omega$ are even smaller. Most interestingly, the $\mathcal{J}^{(2)}$-moment changes at the same time only from 84.71 to 84.84 $\hbar^2$ MeV^{-1}. In view of the fact that the calculations for M=604 are a factor of five slower than those for M=306, we consider it reasonable to keep the latter size of the basis in all calculations presented.

B. Calculations of the dynamical moments

An important advantage of using the HO basis consists in the fact that a rather small number of iterations is sufficient to obtain a high level of convergence. For example, in the case of the yrast configuration in ^{151}Tb at $\hbar\omega$=0.6 MeV, starting from the rotating WS state and performing 50 iterations is enough to obtain the total energy accurate up to 0.5 keV. For all values of rotational frequency and with the same number of iterations performed, the relative precision remains comparable to the one cited above.

This is very important for the calculation of the second moment of inertia $\mathcal{J}^{(2)}$. This quantity has to be calculated by a numerical differentiation, either of the average angular momentum I [42],

$$I = \langle \Psi^\omega | \hat{I}_y | \Psi^\omega \rangle, \tag{4.1}$$

with respect to the rotational frequency ω, Eq. (1.1), or of the total energy $\mathcal{E}$,

$$\mathcal{E} = \langle \Psi^\omega | \hat{H} | \Psi^\omega \rangle, \tag{4.2}$$

with respect to ω:

$$\mathcal{J}^{(2)} = \frac{1}{\omega}\frac{d\mathcal{E}}{d\omega} + \left(\langle \hat{Q}_{20} \rangle - \bar{Q}_{20}\right) \frac{2C_2}{\omega} \frac{d\langle \hat{Q}_{20} \rangle}{d\omega}, \tag{4.3}$$

where the cranking wave functions $|\Psi^\omega\rangle$ are obtained from the HF variational equation

$$\delta \langle \Psi^\omega | \hat{H} + C_2 \left(\langle \hat{Q}_{20} \rangle - \bar{Q}_{20}\right)^2 - \omega \hat{I}_y | \Psi^\omega \rangle = 0. \tag{4.4}$$

In order to obtain accurate values for $\mathcal{J}^{(2)}$, the relative errors of I and $\mathcal{E}$ as functions of ω should be kept as small as possible. The difference of values of $\mathcal{J}^{(2)}$ calculated from Eqs. (1.1) and (4.3) is a measure of self-consistency of solutions. In our example, the previously quoted value of $\mathcal{J}^{(2)}$=84.71 $\hbar^2$ MeV^{-1} has been obtained from Eq. (1.1), while at the same time Eq. (4.3) gives $\mathcal{J}^{(2)}$=84.66 $\hbar^2$ MeV^{-1}. These results have been obtained from the first-order finite-difference approximation of derivatives between $\hbar\omega$=0.60 and 0.61 MeV. Together with the discussed uncertainties related to the restricted size of the basis, these values indicate that our calculated dynamical moments are accurate to about 0.1 $\hbar^2$ MeV^{-1}, which is generally a higher precision than that presently available for the experimental values of $\mathcal{J}^{(2)}$.

C. Quadrupole constraint

The SD states are localized in the pocket of the potential energy surface which is several MeV above the main minimum. When the HF equations are solved by the standard iteration procedure [43], which we also use in our calculations, the wave functions may become gradually polluted by components of the solutions residing principally in the main well, and this may slow-down or even preclude any convergence to the secondary minimum. In order to prevent this kind of effects we have included in the minimized functional a quadratic constraint on the quadrupole moment [44], i.e., we minimize

$$\mathcal{E}' = \mathcal{E} + C_2 \left(\langle \hat{Q}_{20} \rangle - \bar{Q}_{20} \right)^2 \tag{4.5}$$

with a small stiffness parameter C_2=0.01 MeV/b^2 and the constraint value of $\bar{Q}_{20}$=42 b. This is a very weak constraint which has no visible effect on the self-consistent values of the quadrupole moment. It shifts, however, the normal-deformed-minimum energy sufficiently high, so that it does not present any undesired competition with the SD one.

The quadrupole constraint is at the origin of the second term in Eq. (4.3), which compensates for the fact that the quadratic constraint adds to the functional a term which depends on the rotational frequency. The magnitude of this second term depends on the variations of the average quadrupole moment

$$\langle \hat{Q}_{20} \rangle = \langle \Psi^\omega | \hat{Q}_{20} | \Psi^\omega \rangle \tag{4.6}$$

along the rotational band (see Sec. V) and on the difference between $\langle \hat{Q}_{20} \rangle$ and the target value $\bar{Q}_{20}$. In the present calculations this term can be for some bands as large as $0.5\,\hbar^2\,\mathrm{MeV}^{-1}$, and, therefore, cannot be neglected when comparing the values of $\mathcal{J}^{(2)}$ calculated from Eqs. (1.1) and (4.3).

V. THEORETICAL RESULTS AND COMPARISON WITH EXPERIMENT

In this section we present the results of the HF calculations of the multi-band excitation structure of the ^{151}Tb nucleus. In several cases the cross-check results based on the deformed potential of the WS form will also be presented. We divide this discussion into several steps: Secs. V A and V B are devoted to the analysis of the rotational bands in terms of the single-particle Routhians, total energies, and dynamical moments $\mathcal{J}^{(2)}$, while the next ones present problems related to exit spins, shape changes along the rotational bands, and pairing.

A. Superdeformed yrast band in ^{151}Tb

Most probably, only the lowest energy SD bands are populated in the present-day experiments on the SD nuclei. More precisely, the bands lying not too high in the energy scale, at spins between, roughly, 60 $\hbar$ and 80 $\hbar$, can actually be detected. Unfortunately not much more can be said about the population selectivity and no rules for, for instance, the population probability as a function of the actual configuration have been established. Under these circumstances the only way of performing a systematic theoretical analysis consists in calculating numerous bands in excess of the number of those actually measured and in proceeding with a more detailed and critical selection analysis next.

1. Single-nucleonic energy spectra

As the first step the single-particle spectra of the deformed WS cranking Hamiltonian, cf. Sec. III, have been calculated as functions of the cranking frequency for $\hbar\omega$ ranging from 0 to 1 MeV for a few points corresponding to the typical quadrupole $\alpha_{20} \sim 0.58$ and the hexadecapole $\alpha_{40} \sim 0.10$ deformations known to represent well, on the average, the SD nuclei in the $A\sim150$ mass range. Knowing those levels, we define the reference configuration that corresponds to the lowest-level occupation scheme for possibly largest $\hbar\omega$ range. The symbols of the particle-hole configurations used below refer to such a specific reference configuration as the underlying structure. It is worth mentioning that often more than one configuration could quite well serve as the reference and that the actual choice of such a configuration is a matter of commodity. In fact, an inconvenient choice of the reference would merely result in a more complicated labeling of the excited bands: a 1-particle 1-hole excitation with respect to a given reference configuration may become 2-particles 2-holes, 3-particles 3-holes etc. excitation with respect to the inconveniently chosen reference.

In the present analysis we consider Hamiltonians having two discrete symmetries: the parity $\hat{\pi}$ and the y-signature $\hat{R}_y$

$$\hat{R}_y = \exp(-i\pi\hat{I}_y), \tag{5.1}$$

which has the eigenvalues $r{=}{+}i$ or $r{=}{-}i$. The reference of our choice is defined in terms of four types of the occupation numbers: N_{++}, N_{+-}, N_{-+} and N_{--} referring to positive-parity and signature $r{=}{+}i$, positive-parity and signature $r{=}{-}i$, etc., respectively. We have two sets of such numbers for protons and neutrons each. In ^{151}Tb the self-consistent solution for the reference configuration is defined by occupying the single nucleonic orbitals according to the following scheme

$$\begin{aligned} \text{Neutrons:}\ & N_{++} = 22,\ N_{+-} = 22, \\ & N_{-+} = 21,\ N_{--} = 21, \\ \text{Protons:}\ & N_{++} = 15,\ N_{+-} = 16, \\ & N_{-+} = 17,\ N_{--} = 17. \end{aligned} \tag{5.2}$$

In Fig. 1 we show the single-particle Routhians for protons and neutrons obtained with the SkM* [45] parametrization of the Skyrme interaction for the reference configuration given in Eq. (5.2). All HF calculations are in the present study performed using the complete Skyrme functionals, cf. discussion in Ref. [8].

Let us remark that the interpretation of the experimental SD ^{151}Tb(1) yrast band in terms of the configuration implied by relations (5.2) corresponds to the occupation of all the lowest-lying proton Routhians with the last orbital occupied $\pi[6,5,1]3/2(r{=}{-}i)$ (at large ω taking another label: $\pi[6,4,2]5/2(r{=}{-}i)$, cf. Fig. 1). This reference configuration has the lowest calculated total energy at a fixed spin, and therefore, from the theoretical point of view, we can call it the yrast SD configuration in this nucleus. Configuration assignment (5.2) is confirmed by experimentally observed band similarities between ^{151}Tb(1) and ^{150}Gd(2), whose several transitions correspond as being nearly identical. Indeed, this observation can be viewed as a direct consequence of exciting the last occupied proton orbital, $\pi[3,0,1]1/2(r{=}{+}i)$ in ^{150}Gd(2), into $\pi[6,5,1]3/2(r{=}{-}i)$, the last occupied proton level in

^{151}Tb(1). Since the alignment properties and the $\mathcal{J}^{(2)}$-contributions originating from the $\pi[3,0,1]1/2(r{=}{+}i)$ orbital are known to be negligible, Refs. [46,47,8], the assignments of both configurations in the two nuclei can be viewed as confirmed.

In order to establish the uncertainty margin due to various parametrizations of the interactions that have been used in the literature, the results analogous to those in Fig. 1 but for the SIII parametrization of Ref. [48] are presented in Fig. 2. One can see that the characteristic gap structures for the protons (in the form of the sequence of gaps at $Z = 66$, $Z = 64$, and $Z = 62$ visible in Figs. 1 and 2) are very similar in both parametrizations. These gap structures are defined by very similar positions of the $\pi[6,5,1]3/2$ and $\pi[3,0,1]1/2$ orbitals. Other proton orbitals, lying above and below those gaps, differ only slightly in the level ordering. The differences at $\omega = 0$ in the level positions do not exceed typically ~ 500 keV.

It will be instructive at this point to compare the single-particle spectra obtained by using the HF method with the analogous results obtained by making use of the deformed WS cranking Hamiltonian. For this purpose the three-dimensional total-Routhian surfaces for the ^{151}Tb have been calculated in function of the quadrupole (β,γ) and hexadecapole (β_4) deformations, cf. Sec. III A. The total-Routhian surfaces have been calculated in function of the rotational frequency and the minimum-deformation path composed of sets of (β,γ,β_4)-deformation parameters that vary with increasing $\hbar\omega$ has been found. The deformed WS cranking single-particle spectra obtained in this way are presented in Fig. 3.

Let us observe by comparing Figs. 1, 2, and 3, that the global features of the single-nucleon spectra obtained by making use of the deformed average field model with the WS Hamiltonian and those of the HF with the SkM* and SIII interactions are quite similar. What is perhaps most striking is the fact that the WS Hamiltonian and the HF method with the SIII parametrization give very similar single-nucleonic levels indeed. The similarities are particularly well visible in the neutron spectra in Figs. 1 and 3, and only to a slightly lesser extent in the proton spectra displayed in the Figures. This observation can be interpreted in favor of both techniques that employ the two different average fields thus increasing our confidence in the implied results of the microscopic calculations.

2. The $\mathcal{J}^{(2)}$-moments

Since the exit spins of most SD bands are not known, at present the only possible way of testing the calculated $\mathcal{E}$ versus I relation by experiment consists in comparing the resulting $\mathcal{J}^{(2)}$-moments. Before proceeding systematically with such comparisons some additional comments will be useful. We begin by discussing the WS calculations which have been performed here using the so-called "universal" parameters. The corresponding parameter set has been introduced in Ref. [27], and later tested in many detailed calculations of the high-spin properties in nuclei. The corresponding parametrization of the central part of the WS potential employs the radius-parameter values of $r_0(\nu) = 1.347\,\mathrm{fm}$ and $r_0(\pi) = 1.28\,\mathrm{fm}$ for the neutrons and protons, respectively. Historically, these parameter values have been fitted to improve the quality of the single-particle level spectra rather than to reproduce well the geometrical properties of nuclei, and it happens that they exceed considerably the more commonly accepted "geometrical" value of $r_0 \simeq 1.24\,\mathrm{fm}$.

One of the direct implications of the above difference is that the kinematical moments of inertia $\mathcal{J}^{(1)}$,

$$\mathcal{J}^{(1)} = \frac{I}{\omega}, \tag{5.3}$$

calculated from, e.g., the Fermi-gas model with the geometry defined by using the above radius-parameter values systematically exceed the rigid-body moments of inertia calculated from the classical formula with the standard nuclear matter density. Within a classical but also within a semiclassical model, the moments of inertia simply scale with the square of the radius parameter, r_0^2. As a result one should expect that the moments of inertia in various bands, calculated by using the "universal" parametrization of the WS Hamiltonian will be, on the average, too large. We can see that such an expectation, valid for the kinematical moments will apply directly to the dynamical moments (1.1),

$$\mathcal{J}^{(2)} = \frac{dI}{d\omega} = \mathcal{J}^{(1)} + \omega \frac{d\mathcal{J}^{(1)}}{d\omega}, \tag{5.4}$$

and a scaling of the $\mathcal{J}^{(1)}$-moments implies a similar scaling of the $\mathcal{J}^{(2)}$ ones.

By scaling the calculated $\mathcal{J}^{(1)}$ and $\mathcal{J}^{(2)}$-moments we should, as a consequence, also scale the related physical quantities: rotational frequency, energies and Routhians. One can see this after noticing that the scaling of the $\mathcal{J}^{(1)}$ moment with a factor f, that satisfies relation (5.3), for the quantized angular momenta $I = 0, 2, 4, \ldots$ (which remain independent of any scaling), implies the necessity of scaling the rotational (cranking) frequency by a factor of f^{-1}. It then follows that the energies and Routhians also scale as f^{-1}, so as to consistently satisfy the canonical relation $E = R + \hbar\omega I$.

The results of the calculations of the $\mathcal{J}^{(2)}$ moment for the reference (in this case coinciding with the yrast) configuration of ^{151}Tb are given in Fig. 4, where the WS and HF curves are compared with experimental data. Top part of the Figure gives results with no scaling applied. One can see, that the calculated values systematically exceed the experimental ones. In the WS case we know that, as mentioned above, the numerical values of the radius-parameters are too large and we can clearly consider at least a part of the discrepancy as related to "too large a volume of the nucleus". Therefore, in the bottom part of Fig. 4 we show the same $\mathcal{J}^{(2)}$-moments scaled by the factor f=0.9.

In the HF case there is no obvious discrepancy between the calculated and experimental nuclear radii. Nevertheless, the calculated $\mathcal{J}^{(2)}$-moments as well as quadrupole moments are systematically slightly too large (see Refs. [49,50] for recent measurements of the quadrupole moments and Ref. [51] for the results of systematic HF calculations of the quadrupole moments and comparison with experiment). Such an overestimation is consistently obtained for many different Skyrme force parameters [8]. At present, no explanation of this systematic effect can be found. For the sake of the presentation we have therefore decided to use the same phenomenological scaling factor f=0.9 to present the results of HF calculations.

This scaling procedure, as we have checked by an explicit comparison with the experimental results, works well for all the bands in the ^{151}Tb nucleus simultaneously. Moreover, we have checked that by using the same scaling factor f=0.9 for many bands and for several nuclei simultaneously one reproduces well the experimental $\mathcal{J}^{(2)}$ moments which otherwise remain too large. This conclusion is based on comparisons for the yrast bands in ^{151}Dy,

^{152}Dy, ^{153}Dy, ^{149}Tb, and ^{150}Tb, and also for a few dozens of excited SD bands in the mass $A\sim150$ region. Light Gadolinum nuclei (^{146}Gd and ^{147}Gd) have strong alignment effects in their yrast SD bands and are not well suited for the tests discussed here. Slopes of the $\mathcal{J}^{(2)}$ moments in ^{148}Gd, ^{149}Gd, and ^{150}Gd are overestimated in the calculations; for the discussion of the latter nucleus see Sec V E. Conversely, not introducing the aforementioned scaling we find the calculated values systematically too high, by 8 to 10%.

After applying the scaling procedure according to the discussion above, (cf. Fig. 4 for illustration), the $\mathcal{J}^{(2)}$-moments are multiplied by the factor of f and the angular frequencies by a factor of f^{-1}. Then, a very good correspondence with the ω dependence of the experimental data is worth noticing. Below we present all results scaled according to the prescription and parameters defined above. Let us mention that no physical conclusion of this paper depends on using or not using the scaling procedure described above; the scaling can be viewed as merely a "graphical" trick to facilitate a comparison with the experimental data. Moreover, we have not attempted any detailed fit of the scaling factor f=0.9 which can still be varied within about ±0.02 without any obvious general deterioration of the agreement with data.

B. Excited SD bands in ^{151}Tb

The problem of the definition of the yrast configuration discussed in Sec. V A 1 did not pose any serious difficulty. Firstly, in nuclei with the nucleon numbers in the vicinity of large SD gaps (as e.g. Z=66 and N=86) the yrast configurations corresponding to the occupation of the lowest-lying levels are relatively easily and unambiguously determined over a relatively long ω-range since no, or very few level crossings occur at the Fermi level (cf. Fig. 1). Secondly, the experimentally dominating SD band (i.e., the one with the highest population intensity) is also easily distinguished. In the case of the other SD bands neither of the observations applies. In experiment several bands are populated with comparable (usually weak) intensities and their relative excitation energies are totally unknown. In theory, numerous close lying bands remain *a priori* the candidates for a much smaller number of the experimental bands to be associated with.

Moreover, the uncertainties in the relative positions of the theoretically calculated levels which sometimes influence the level ordering may reach 500 keV or more. This estimate corresponds to a typical discrepancy between the results obtained within commonly used average field models (like WS potential or Skyrme interaction parametrizations, SkM* and SIII as discussed above and illustrated in Figs. 1, 2 and 3) and may, occasionally, become markedly larger. Consequently, in analyzing the structure of the nucleus in question we have applied the following approach:

(i) Our primary goal in this section is to recognize within the applied formalism the most probable single-nucleonic (particle-hole) structure that underlies the behavior of the experimentally found bands.

(ii) We are using, for the sake of *qualitative* argumentation, the calculated ordering of various SD bands: the lower the band energy at the *high-spin limit*, the higher the chance to find such a band among those populated in experiment.

(iii) We use the experimental $\mathcal{J}^{(2)}$-moments and verify the possible single-nucleonic configurations by directly comparing $\mathcal{J}^{(2)}(\omega)$ with experiment.

Another important piece of information suitable for identifying single-particle configurations is the sameness of bands in different nuclei, i.e., the equality of the corresponding dynamical moments and specific relations which occur for the relative alignments, see the review in Ref. [13]. In the present work we mainly use and analyze the properties of the dynamical moments, because those of the relative alignments are very sensitive to the details of the effective interactions [8]. A readjustment of the interaction parameters, especially those related to time-odd components of the mean field, seems to be necessary for a precise theoretical determination of the relative alignments.

In order to apply the guidelines (ii) and (iii) above, we first present the results for the lowest-lying one-particle one-hole excited bands. In Figs. 5 and 6 we show the total energies for the proton and neutron excitations, respectively. Here and in the following we label the configurations by the corresponding Nilsson labels of hole and particle states, as well as by the total parity and signature quantum numbers supplemented by (arbitrary) consecutive number attached to each configuration. Since in ^{151}Tb the size of the proton shell gap is smaller than that for the neutrons, there are more low-lying proton than neutron excited bands. Since we know that there exist uncertainties in the single-particle level positions that may influence the relative positions of some bands in a non-negligible manner, the results in Figs. 5 and 6 should be treated as a semi-quantitative guide. The Figures show 10 proton particle-hole and 12 neutron particle-hole excited bands, respectively, that appear to be the lowest at $I \sim 80\hbar$, i.e., in the spin range where the superdeformed bands are populated. We have placed some of the curves in the upper parts, and some others in the lower parts of the Figures trying to illustrate an existence of "families" of bands, each family characterized by some specific features like slopes or band crossings. In the case of neutrons, the separation into two families is particularly well visible. The differences in this case (cf. also Figs. 7 and 8) correspond to the structure differences in the two characteristic hole-orbitals ($\nu[6,5,1]3/2(r{=}{+}i)$ or $\nu[6,5,1]3/2(r{=}{-}i)$, top parts, and $\nu[7,6,1]3/2(r{=}{-}i)$ bottom parts).

Figures 7 and 8 present the theoretical predictions for the dynamical moments corresponding to the bands shown in Figs. 5 and 6, respectively. One can see that the theoretically calculated moments form "families" characterized by a similar behavior also in the proton case. In particular the bands built on the configurations of the type $\pi[3,0,1](r{=}{\pm}i)$ $\rightarrow$ $\pi[6,6,0](r{=}{+}i)$ and $\pi[6,5,1]3/2(r{=}{-}i)$ $\rightarrow$ $\pi[6,6,0](r{=}{+}i)$ are characterized by similar slopes, in terms of the $\mathcal{J}^{(2)}$ moments; these slopes are different from that of the reference band. On the neutron side, the similarities between the bands related to exciting the $\nu[7,6,1]3/2(r{=}{-}i)$ orbital into the orbitals $\nu[5,1,4]9/2(r{=}{\pm}i)$, $\nu[5,2,1]3/2(r{=}{\pm}i)$, and $\nu[4,0,2]5/2(r{=}{\pm}i)$ deserve noticing. Distinguishing among these properties will be particularly useful when attributing the configurations to the experimental bands since, as mentioned before, several theoretical configurations provide similar $\mathcal{J}^{(2)}$ moment dependence on the rotational frequency, while their energies are also quite close.

1. Bands $^{151}Tb(2)$, $^{151}Tb(3)$, and $^{151}Tb(4)$

We proceed with the interpretation of the experimental results for Bands 2, 3, and 4. Although the most likely structures of these bands have already been discussed before in the literature [46,23,9,12], we found it instructive to illustrate the procedure of attributing the

theoretical bands to the experimental ones, the procedure which will be of more importance for other bands for which an adequate interpretation remains less easy.

By eliminating the bands whose $\mathcal{J}^{(2)}$-moments differ relatively strongly with respect to the experimental result for Bands 2-4, we arrive at a comparison presented in Fig. 9. Here and in the following we denote the HF states by their dominant Nilsson labels at *high frequencies*, cf. Fig. 1. For example, the above mentioned $\pi[6,6,0]1/2(r{=}{+}i)$ Routhian originates at low frequencies from the $\pi[6,5,1]3/2(r{=}{+}i)$ state.

Experimental results for Bands 2 and 4 agree rather well with calculations for configurations based on exciting either of the signature partners of the $\pi[3,0,1]1/2(r{=}{\pm}i)$ orbitals into the $\pi[6,6,0]1/2(r{=}{+}i)$ state. As seen in Fig. 5, the configuration based on the $\pi[3,0,1]1/2(r{=}{+}i)$ Routhian has the energy lower by about 1 MeV than that based on the corresponding signature partner, and therefore the former should be retained as the most likely interpretation of Band 2. Similarly, the dynamical moment of the $\pi[6,5,1]3/2(r{=}{-}i)$ $\rightarrow \pi[6,6,0]1/2(r{=}{+}i)$ configuration, Fig. 9, middle part, reproduces very well the data for Band 3, and this supports the corresponding interpretation (proposed also in Ref. [23]). The suggestion of this configuration is based simultaneously on the fact that it corresponds to a low-energy excitation, as it is seen from Fig. 5, and that it provides a good agreement of the $\mathcal{J}^{(2)}$ versus ω dependence with the experimental one.

On the other hand, as seen in Figs. 1, 2, and 3, all calculations give at high frequencies the low-lying Routhian $\pi[5,3,0]1/2(r{=}{+}i)$ that might produce configurations which are lower in energy, cf. Fig. 5, bottom part, than those based on excitations to the $\pi[6,6,0]1/2(r{=}{+}i)$ state (cf. also Fig. 7, bottom part).

2. *Bands* $^{151}Tb(5)$ *and* $^{151}Tb(6)$

The experimental results for bands ^{151}Tb(5) and ^{151}Tb(6) indicate a correlation with the yrast sequence of the isotope ^{150}Tb [22]. This suggests that the neutron Routhian $\nu[7,7,0]1/2(r{=}{-}i)$, cf. Figs. 1 and 3, is not occupied in the related configurations. [Due to the level interactions at large ω-values the label of this level changes into $\nu[7,6,1]3/2(r{=}{-}i)$]. Indeed, calculations indicate that several neutron particle-hole excitations give the required dependence of $\mathcal{J}^{(2)}$ versus ω, as seen in Fig. 8. These are excitations from the $\nu[7,6,1]3/2(r{=}{-}i)$ orbital to either of the $\nu[4,0,2]5/2(r{=}{\pm}i)$, $\nu[5,2,1]3/2(r{=}{\pm}i)$, or $\nu[5,1,4]9/2(r{=}{\pm}i)$ orbitals. A comparison of the dynamical moments corresponding to the configuration $\nu[7,6,1]3/2(r{=}{-}i) \rightarrow \nu[5,2,1]3/2(r{=}{\pm}i)$ is given in Fig. 10 as an example, while the excitation energies are presented in Fig. 6. One can see that the energies of the latter configurations are $\sim$ (600 to 800) keV higher than those of the former ones, thus favoring the involvement of the neutron $\nu[4,0,2]5/2$ and $\nu[5,2,1]3/2$ orbitals as a more likely explanation.

3. *Bands* $^{151}Tb(7)$ *and* $^{151}Tb(8)$

The experimental results for bands ^{151}Tb(7) and ^{151}Tb(8) indicate a correlation with the yrast band in the ^{149}Gd nucleus [22]. Such a correlation suggests that the last proton intruder level, $\pi[6,4,2]5/2(r{=}{-}i)$, remains unoccupied with the corresponding proton on a low lying orbital with a small $\mathcal{J}^{(2)}$-contribution. In fact, the low-lying $\pi[5,3,0]1/2(r{=}{+}i)$

orbital visible, e.g., in Fig. 1 provides an excellent result, cf. Fig. 11. However, since a pair of degenerate bands is seen in the experiment, one should also consider some other possibilities. In fact, several neutron configurations mentioned in the preceding Section remain equally good candidates, and in Fig. 11 we also present a comparison with the experiment of the results obtained for the $\nu[7,6,1]3/2(r{=}-i) \rightarrow \nu[4,0,2]5/2(r{=}\pm i)$ excitations.

It is important to observe that the similarity between the $\mathcal{J}^{(2)}$-moments in ^{149}Gd(1), and those in the ^{151}Tb(7,8) bands is accompanied by noticeable differences in both the Q_{20} and Q_{40} moments calculated for the bands with the configurations mentioned. For instance the proton excited configuration carries about 0.5 b more than the neutron one: $Q_{20}[\pi(651)3/2 \rightarrow \pi(530)1/2] > Q_{20}[\nu(761)3/2 \rightarrow \nu(402)5/2]$, as it is seen in Fig. 11.

For the bands ^{151}Tb(7) and ^{151}Tb(8) we thus have three possible configurations which give almost indistinguishable dynamical moments. The importance of the above example lies in the fact that the configurations for rather different quadrupole moments and/or deformations may still lead to very similar dynamical moments. Therefore, a direct association of "identical" quadrupole moments and "identical" dynamical moments is not supported by microscopic calculations. The bands having identical dynamical moments may still carry quite different deformations and/or quadrupole moments.

C. Predictions related to spins in the superdeformed bands of ^{151}Tb nucleus

The problem of the exit spins in SD bands is one of the most actual in the present-day studies of the nuclear superdeformation. Many questions remain half-answered since the connections between the SD bands and the rest of the nuclear decay schemes are not known in the $A{\sim}150$ nuclei from the experimental point of view. This makes it impossible to measure, e.g., the absolute alignments or $\mathcal{J}^{(1)}$-moments, and to estimate the degree to which the rapid nuclear collective rotation resembles that of a rigid body. Such questions are being posed also in relation to the pairing behavior at high spins and in many other contexts.

Our calculations allow, in principle, to predict the absolute (and thus also the relative) exit spins of the SD bands studied. In practice, however, there are some deficiencies of (all) the methods used which impose limitations on the predictive power related to these particular results of calculations.

First of all, in our HF calculations the pairing correlations have been neglected and the obtained results concerning the alignment effect may introduce at least small uncertainties. Although it is often believed that the spins calculated at a given cranking frequency ω must be lower when the pairing correlations are included, the actual tendency will depend on the position of the Fermi level relative to the occupation of the large-j shells: the down-sloping (beginning of the shell) and the up-sloping (upper part of the shell) orbitals contribute to the total alignment in opposite ways. Several aspects related to pairing will be presented in Sec. V E.

We have analyzed the calculated spin versus frequency plots for all the bands studied in this article. The experimental spins of the last levels seen experimentally are not known. Therefore, we can only compare the theoretical and experimental *differences* of spin along the calculated and observed bands. To this end, we define the theoretical difference of spin as

$$\Delta^{\rm th} I = I^{\rm th}(\omega) - I^{\rm th}(\omega_{\rm o}) + 2\hbar, \tag{5.5}$$

where $\omega_{\rm o}$ is calculated from the two lowest experimental transitions according to the standard expression (2.1a). This theoretical difference can be compared to the experimental difference of spin

$$\Delta^{\rm exp} I = I^{\rm exp} - I^{\rm exp}_{\rm o} + 2\hbar = 2n\hbar, \tag{5.6}$$

(as a function of ω) relative to the (unknown) spin $I^{\rm exp}_{\rm o}$ of the state fed by the lowest transition seen in experiment. This experimental difference of spin simply equals twice the number n of the gamma transition counted from the bottom of the band. A shift of $2\hbar$ is added to both definitions (5.5) and (5.6) to account for the fact that the lowest experimental value of the frequency (2.1a) ($\omega_{\rm o}$) is known at $I^{\rm exp}_{\rm o}+2\hbar$.

For all the SD bands in ^{151}Tb, calculated within the HF method using the SkM* force and with the scaling factor f=0.9 discussed in Sec. V A 2, the differences between $\Delta^{\rm th} I$ and $\Delta^{\rm exp} I$ do not exceed $1\,\hbar$, for all the frequencies studied, i.e., from 0.3 to 0.9 MeV/$\hbar$. The same is also true (up to $0.5\,\hbar$) for the yrast band in ^{152}Dy. On the other hand, similar comparison gives a disagreement for the yrast band in ^{150}Gd, which indicates a necessity to consider the pairing correlations in this nucleus, see Sec. V E.

The spins calculated at $\omega_{\rm o}$ give predictions for the exit spins $I_{\rm o}$ in the SD bands,

$$I_{\rm o} = \left[I^{\rm th}(\omega_{\rm o})\right] - 2\hbar, \tag{5.7}$$

where the brackets [ ] denote the rounding to the nearest integer or half-integer compatible with the total signature and the parity of the number of particles. The obtained values of $I_{\rm o}$ are collected in Table II together with the summary of the theoretical HF configurations used. In some cases where clearly more than one configuration may be considered, two of them are included in the Table to illustrate the possible uncertainty of the configuration.

The results for the $I_{\rm o}$-values have been given in the Table as differences with respect to the $I^{(1)}_{\rm o}$=69/2 $\hbar$ value obtained for Band 1 which is used as the reference. The representation in terms of differences is used to stress that the absolute value of $I^{(1)}_{\rm o}$ may be considered less certain (given the uncertainties of the scaling procedure, neglect of pairing, etc.) as compared to relative alignments between different bands, which are expected to be much less model dependent. For example, the exit spin obtained in ^{152}Dy(1) from the HF calculations without pairing is $I_{\rm o}$=26 $\hbar$ (for the state fed by the 602.4 keV transition). This is fully compatible with the exit spin of 57/2 $\hbar$ obtained in band ^{151}Tb(2) (for the next transition of 646.5 keV) and giving the relative alignment of +1/2 $\hbar$, cf. Ref. [8].

The effects of dynamical correlations caused by pairing on the alignment mechanism in SD bands of the neighboring nucleus ^{152}Dy have been studied, e.g., in Ref. [16]. These effects are expected to be small, of the order of a few $\hbar$ at the most, and to be rather regular functions of the frequency. The corresponding alignment corrections were calculated to be negative for several bands in the $A\sim$150 nuclei. We have repeated the analysis of these correlations for the even-even neighbors of ^{151}Tb, i.e., for ^{152}Dy and ^{150}Gd, for which the pairing effects are not influenced by the blocking mechanism, and are easier to extract in a relatively pure form (cf. Sec. V E).

Without pairing, the same value of $I_{\rm o}$=26 $\hbar$ is for ^{152}Dy(1) obtained both within the HF and WS calculations. As shown in Sec. V E, the inclusion of pairing in the WS method

brings this value down to $24\,\hbar$. Because the pairing influence increases from ^{152}Dy towards ^{150}Gd, we can very tentatively estimate that the HF absolute exit spins in Terbium obtained without pairing overestimate the values with pairing by about $4\,\hbar$. Hence the inclusion of pairing would give the exit spin of $I_\circ^{(1)}$=61/2 $\hbar$ for the state fed by the 768.4 keV transition in the ^{151}Tb(1) band.

It is important to observe that the obtained exit-spin values vary rather markedly from band to band. In particular, in ^{151}Tb(1) the value of $I_\circ$ is significantly larger (by $6\,\hbar$) than that predicted for the first excited band ^{151}Tb(2).

D. Shape evolution with spin

The shape evolution for various configurations studied in this article has been determined by calculating the expectation values of the quadrupole moments, Q_{20} and Q_{22}, and the hexadecapole moments Q_{40}, Q_{42}, and Q_{44} [41]. The calculated axial quadrupole and hexadecapole moments, Q_{20} and Q_{40}, decrease with increasing rotational frequency for all the bands studied. The corresponding results for the most important proton moments, i.e., Q_{20} and Q_{40} are presented in Fig. 12. In Fig. 13 we show for each band the proton quadrupole moments in function of the dynamical moments. One can see that these relations are nearly linear, which indicates that the changes in $\mathcal{J}^{(2)}$ are correlated with changes of Q_{20}. One can interpret this characteristic result as a dynamical-moment evolution accompanying the nuclear-shape polarization due to the rotation.

It is also worth observing that the proton excited configurations have noticeably higher quadrupole moments and that their slopes are slightly higher than those of the neutron excited bands.

Slight but systematic deviations from the axiality are predicted with increasing rotational frequency. It is worth mentioning that the deviations from axiality for the signature-partner configurations, π[3,0,1]1/2(r=+i) $\rightarrow$ π[6,6,0]1/2(r=+i) and π[3,0,1]1/2(r=−i) $\rightarrow$ π[6,6,0]1/2(r=+i), attributed to Bands 2 and 4, respectively, have opposite signs, although they both remain small.

The axial hexadecapole moments Q_{40} are relatively diversified in that their variations in function of the configuration and rotational frequency may reach as much as 25%. The more exotic hexadecapole moments with the non-zero μ-components, i.e., Q_{42} and Q_{44}, have also been calculated. The interest in those moments has grown recently in relation with the so-called ΔI=2 staggering observed in transition energies of some rare-earth SD nuclei. The staggering could manifest a presence of those exotic multipoles in the nuclear shapes and in particular, the non-zero Q_{44}-moments could manifest the nuclear C_4-symmetry, as suggested in Ref. [52] and discussed in [53]. The effect in question may be very small, as shown by microscopic calculations [54–58]. Experimentally, the staggering phenomenon has not been reported to exist in ^{151}Tb nucleus. Nevertheless, we found it of interest to estimate the order of magnitude of the relevant hexadecapole moments. The calculations indicate that the Q_{42}-moments, although typically two orders of magnitude smaller than the Q_{40}-moments, remain non-zero, while the Q_{44}-moments are still at least by a factor of a few smaller.

E. The moments of inertia in the presence of pairing

The main purpose of the scaling procedure introduced in Sec. V A 2 was, on the one hand, to quantify the systematic deviations from the experiment of the obtained results for the $\mathcal{J}^{(2)}$-moments. On the other hand this procedure proves indeed that the obtained discrepancies are systematic since the same scaling factor has been successfully used in various nuclei (and for all the bands known in each of them). The comparisons were made for several dozens of bands; presentation of these results was limited so far in this paper to 8 bands in ^{151}Tb only. Discrepancies of similar order of magnitude were also present in calculations of other authors, but were not discussed in any major detail. Only as a result of an extended comparison with the experimental data we were lead to a suggestion that the discrepancies are systematic and thus that the underlying theories (or parametrizations of the forces) might be, and most likely should be improved.

As it is well known, the pairing correlations influence the moments of inertia in a rather characteristic manner. Typically (although not generally), the stronger the pairing correlations, the smaller the kinematical moments $\mathcal{J}^{(1)}$. The purpose of the present Section is to estimate the effect of pairing on the discussed moments, thus putting more restriction on the uncertainties produced by the applied nuclear effective forces.

A technique used here differs from those of Refs. [15] and [9] in that we perform the particle number projection (PNP) of the rotating BCS type wave functions *before* variation (in the former publication the RPA technique within the Nilsson model has been used while in the latter, an approximate projection in terms of the Lipkin-Nogami method together with the HFB approximation). Here we apply the pairing-self-consistent Bogolyubov method and the PNP before variation, using the standard monopole pairing Hamiltonian with the constant average matrix elements, different for the protons and the neutrons (see below), and the WS cranking approach.

Calculations [9] of the SD bands in $A\sim150$ nuclei have shown that the inclusion of pairing through the density-dependent zero-range interactions improves the agreement with data in ^{150}Gd, but at the same time the agreement in ^{152}Dy is destroyed. It seems therefore, that at present one needs some more effort, also in the case of the HF approach, to clarify the problem of the effective interactions used, and although here we will not be able to carry through such a complex project, we would nevertheless like to quantify the difficulty and prepare the starting point for a more advanced discussion.

Below we are going to concentrate on the two neighbor-isotones of the $^{151}\mathrm{Tb}_{86}$ nucleus, i.e., $^{150}\mathrm{Gd}_{86}$ and $^{152}\mathrm{Dy}_{86}$. We believe that studying the two even-even nuclei has, in the present context, some important advantages. As our calculations, as well as those of other authors indicate, in the isotones in question the main pairing contributions come from the N=86 neutron system. Since the relative proton/neutron pairing strengths are uncertain, in studying the weak pairing limit, the two even-even nuclei mentioned offer less uncertainties as compared to odd-A ones in which the blocking in the case of the odd proton may cause an additional difficulty. In other words: it is not known at present whether at the weak pairing limit that we are confronted with at high spins the usual blocking procedure is a sufficient an approximation.

In order to estimate the influence of the pairing on the alignment process, we have calculated the kinematical and dynamical moments in function of rotational frequency at fixed

deformations representing the average equilibrium-deformation values for the two nuclei in question (for details see captions to Figs. 14 and 15). We have taken N and Z single-particle states into account when constructing the Bogolyubov transformation for neutrons and protons, respectively. When parametrizing the pairing constants (average matrix elements) we took as a starting point the pairing force strength parameters from Ref. [59]

$$G_n = \frac{1}{A}[18.95 - 0.078(N-Z)], \tag{5.8a}$$

$$G_p = \frac{1}{A}[17.90 + 0.176(N-Z)], \tag{5.8b}$$

where they have been adjusted to experimental data on normal nuclei by applying the pairing-self-consistent Bogolyubov formalism without the PNP. When used within the particle projection formalism, these values have to be decreased, by about 15% (several aspects related to the PNP technique can be found in Ref. [60] (solvable model) and, e.g., in Refs. [18,16] (cranking with the WS Hamiltonian)). In the present application we use the reduction factors of 0.85 for both the neutrons and the protons, i.e., we apply $0.85\,G_n$ and $0.85\,G_p$ in the monopole pairing Hamiltonian. In this respect we in fact apply the parametrization studied earlier in the normal nuclei thus not introducing new parameters for those nuclei studied in this paper. The results corresponding to our PNP calculations are presented in Figs. 14 and 15 for the ^{152}Dy and ^{150}Gd nuclei, respectively. Let us observe that the high spin results for the dynamical moments in ^{150}Gd agree very well with experiment. Note that the scaling factor used here, f=0.9, is the same as that applied in the calculations without pairing presented previously. In other words, in this nucleus the calculations without pairing would not agree with the data.

Altogether, similarly as in Ref. [9] the results with pairing correspond to an increase in $\mathcal{J}^{(2)}$ moments as compared to those without pairing. At lower spins the crossing observed in the data through the rise in the $\mathcal{J}^{(2)}$ moments appears at a similar frequency also in the calculations, although the theoretical crossing frequency is slightly too large. In any case such a crossing is to a far an extent a matter of individual level positions rather than the collective pairing phase, and as such is of less importance for the discussion in this Section.

The results for the dynamical moments in ^{152}Dy present similar defect at small frequency limit where the calculation provide a crossing-like structure at frequencies which are slightly too high. Again, for most of the spin values, the dynamical moments obtained with pairing are larger than those without pairing. Consequently, the pairing cannot be a remedy for the too high moments as calculated (without scaling) both within the WS and HF methods.

Concerning the high spin behavior of the dynamical moments (slightly different slopes in theory as compared to the data): we have checked that a shape evolution (ignored in the calculations presented in Figs. 14 and 15) brings in the effects of broad proton crossings whose onsets are already visible in the Routhians from Fig. 3. These effects are present in a form of a slight modification of the $\mathcal{J}^{(2)}$ vs. ω dependence in the experimental frequency range at highest spins only when the proton pairing is taken into account. The aforementioned modification is sufficient to provide the correct asymptotic of the $\mathcal{J}^{(2)}$ at high spins in ^{152}Dy.

Having obtained an overall agreement with the data on the dynamical moments we have also compared the $\mathcal{J}^{(1)}$-moments as well. The agreement of the kinematical moments can be considered very good for both nuclei when the experimental exit-spin values (so far not measured) are assumed to be equal to those calculated according to the method described in

Sec V C, i.e., I_o=24 and 32 $\hbar$ for ^{152}Dy and ^{150}Gd, respectively. Incidentally, without pairing, the same method gives the value of I_o=38 $\hbar$ in ^{150}Gd, and an incorrect behavior for the spin difference $\Delta^{th}I$.

Let us note that by taking into account the pairing correlations a good description of the kinematical moments at the high-spin limit is obtained for the same values of the scaling factor and pairing constants common for both nuclei, although the effects of pairing, especially in the neutrons, are calculated to be markedly different in the two isotones discussed. In all compared situations a scaling factor was necessary in order to bring the too high no-pairing results on the $\mathcal{J}^{(1)}$ and $\mathcal{J}^{(2)}$-moments towards the experimental data simultaneously for both nuclei studied.

For all the three nuclei, i.e., $^{150}Gd_{86}$, $^{151}Tb_{86}$, and in $^{152}Dy_{86}$, the inertia contribution coming from the neutrons is expected to dominate that of the protons by about a factor of two; also the pairing effects are calculated to have about a factor of two more effect in the neutron case. Comparison of the results in the top and the bottom parts of Figs. 13 and 14 indicates that at the highest frequency range the differences between the proton contributions for the case with pairing as compared to the no-pairing case amount to not more than about 1 $\hbar^2$ MeV^{-1} (about 1%) in ^{152}Dy nucleus and about 0.5 $\hbar^2$ MeV^{-1} (about 0.5%) in the ^{150}Gd nucleus. In the case of the neutrons the corresponding differences are slightly larger but also very small and thus the pairing is calculated to influence the kinematical moments at the highest frequency limit by about 3%.

At the low frequency range the pairing correlations are expected to be systematically more important. The effect of pairing at $\hbar\omega \sim 0.4\,MeV$ on the moment of inertia is about 10% in ^{152}Dy and about 20% in ^{150}Gd. The main difference between the calculations for ^{152}Dy and ^{150}Gd is the smaller deformation in the case of ^{150}Gd; the deformations for most of the bands in the ^{151}Tb nucleus are in between those for the discussed even-even isotones. Consequently we should expect that at the low frequency range in the ^{151}Tb nucleus, the pairing correlations should still amount to $\sim$ 15% on the average, those of the protons being negligible for two reasons: firstly they are very small in the two neighboring even-even nuclei and, secondly, the $65th$ odd proton in the ^{151}Tb is expected to diminish the proton pairing effect even more due to the blocking arguments. This is also why the results for the Terbium nucleus are expected to lie in between those for the neighboring even-even nuclei studied here. The detailed analysis of this nucleus calls first, however, for a microscopic justification of the scaling factor introduced in the present study, and for an improved treatment of pairing in an odd nucleus.

There exists of course an uncertainty margin in the above estimates. The dynamical moments are sensitive to the detailed variation of the single-nucleonic Routhians with the rotational frequency and a slow alignment of one single orbital may modify the $\mathcal{J}^{(2)}$ moment considerably thus increasing the risk of estimating the collective pairing effect from the influence of one level. Secondly, it is impossible to experimentally separate the proton and neutron contributions and thus in the calculations one may obtain in principle similar results by increasing, e.g., the proton pairing strength while decreasing that of the neutrons. Fortunately, in the two nuclei discussed the protons contribute significantly less to the total inertia as compared to the neutrons and, in addition, the neutron pairing effects at $N = 86$ in the Dy and Gd isotones differ considerably. Consequently the second uncertainty mentioned has a rather small influence on the final result.

VI. SUMMARY AND CONCLUSIONS

In this article the two most efficient microscopic approaches in the high-spin nuclear structure calculations, i.e., those based on the average nuclear field parametrization in terms of the deformed WS potential and the self-consistent HF approach together with the cranking method have been applied. The results of the calculations employing these two different methods and also the results of the calculations with two different parametrizations of the Skyrme interactions have been compared.

Despite of the fact that the formalisms used differ strongly, the efforts put earlier (by other authors) in optimizing the parametrizations of the interactions seem to converge: the single-nucleon spectra generated by the HF and the WS Hamiltonians are very similar. In particular, we have demonstrated that at least for the nucleus studied the self-consistent HF solutions and the WS-Strutinsky energy minimized results lead to similar super-deformed shell closures. In protons there is a series of shell gaps corresponding to Z=62, 64 and 66 with a characteristic high level-density areas closing those gaps from below and from above. The π[3,0,1]1/2 orbital separates the former two gaps and the π[6,5,1]3/2 orbital the latter two gaps in both SkM* and SIII parametrizations of the Skyrme interaction and in the WS case. Of course in the high-level density areas the relative positions of the single-particle states differ slightly but practically all the same Nilsson orbitals are represented there. In the neutron spectra the N=86 SD gap is cut into two (N=86 and N=85 gaps) by one of the signature partners of the ν[7,7,0]1/2 orbital. The neutron spectra manifest two systematic differences (when comparing HF and WS): (i) the signature splitting of the ν[7,7,0]1/2 orbital is much stronger in the HF approach independently of the force, and (ii) below the big gaps we find, in the decreasing order, the ν[6,4,2]5/2, ν[6,5,1]1/2, and ν[4,1,1]1/2 orbitals; in the WS case these N=6 orbitals are inverted. The inversion, however, did not cause any significant problem in interpretations of the spectra in the ^{151}Tb nucleus.

Theoretical calculations of the dynamical moments indicate a fair or good agreement for eight bands known experimentally in ^{151}Tb. This is possible, however, only after a phenomenological scaling factor, common for all bands, is introduced. Generally, for higher-lying SD bands a unique interpretation of the single-nucleonic structure in terms of the Nilsson labels does not seem possible (at least at present) for several reasons. Firstly, the single-nucleonic Routhian spectra contain levels of different intrinsic characteristics which remain nearly degenerate over the long ranges of rotational frequency. They lead to numerous configurations with very similar alignment and dynamical-moment properties and of very close total energies. Secondly, the band degeneracy (twinned band effect) does not provide major help in such cases since several among excited bands may produce nearly identical band spectra.

The deformation changes in function of the band-configurations and rotational frequency are very characteristic: in all bands discussed not only the quadrupole (Q_{20}) and the hexadecapole (Q_{40}) moments decrease with increasing frequency, as observed also by other authors, but also their variation seems clearly correlated with that of the dynamical and kinematical moments. With progressing alignment small triaxialities (equivalent to the γ-deformations of the order of a few degrees) develop as well.

The possibility of the existence of some special symmetries (like, e.g., an occurrence of the shapes with the C_4-symmetry) has been studied. No indication for the Q_{44}-moments

has been found (an upper limit is predicted at the level of at most $10^{-3} \times Q_{40}$).

The calculations allow to predict the values of the exit spins, i.e., the spins of the lowest observed SD transitions. These predictions are given by the values of spin calculated at the rotation frequency corresponding to the lowest observed transition, and rounded to the nearest half-integer value compatible with the total signature. The differences between the exit-spin values in different bands are expected to be more reliable than the corresponding absolute values.

We found that the systematic discrepancies between the experimental and calculated results exist in both WS and HF approaches, even if the pairing correlations are taken into account. This suggests a need for more effort in determining the optimal parametrizations of the effective interactions used for a description of the high-spin properties of the strongly-deformed nuclei.

ACKNOWLEDGMENTS

We would like to express our thanks to the *Institut du Développement et de Ressources en Informatique Scientifique* (IDRIS) of CNRS, France, which provided us with the computing facilities under Project no. 960333. This research was supported in part by the Polish Committee for Scientific Research under Contract No. 2 P03B 034 08, and by the computational grant from the Interdisciplinary Centre for Mathematical and Computational Modeling (ICM) of the Warsaw University.

REFERENCES

[1] S. Åberg, H. Flocard and W. Nazarewicz, Annu. Rev. Nucl. Part. Sci. **40**, 439 (1990).
[2] T. Werner and J. Dudek, Atomic and Nucl. Data Tables, **59**, 1 (1995).
[3] P. Bonche, H. Flocard and P.H. Heenen, Nucl. Phys. **A467**, 115 (1987).
[4] P. Bonche, H. Flocard and P.-H. Heenen, Nucl. Phys. **A523**, 300 (1991).
[5] B.Q. Chen, P.-H. Heenen, P. Bonche, M.S. Weiss and H. Flocard, Phys. Rev. **C46**, 1582 (1992).
[6] J.L. Egido and L.M. Robledo, Phys. Rev. Lett. **70**, 2876 (1993).
[7] M. Girod, J.P. Delaroche, J.F. Berger, and J. Libert, Phys. Lett. **B325**, 1 (1994).
[8] J.Dobaczewski and J. Dudek, Phys. Rev. **C52**, 1827 (1995).
[9] P. Bonche, H. Flocard, and P.-H. Heenen, Nucl. Phys. **A598**, 169 (1996).
[10] W. Koepf and P. Ring, Nucl. Phys. **A493**, 61 (1989); **A511**, 279 (1990).
[11] J. König and P. Ring, Phys. Rev. Lett. **71**, 3079 (1993).
[12] A.V. Afanasjev, J. König, and P. Ring, Nucl. Phys. **A608**, 107 (1996).
[13] C. Baktash, B. Haas, and W. Nazarewicz, Annu. Rev. Nucl. Part. Sci. **45**, 485 (1995).
[14] T. Bengtsson, I. Ragnarsson, and S. Åberg, Phys. Lett. B **208**, 39 (1988).
[15] Y. R. Shimitzu, E. Vigezzi, R. A. Broglia Phys. Lett. **198B**, 33 (1987); Y. R. Shimitzu, E. Vigezzi, R. A. Broglia Nucl. Phys. **A509**, 80 (1990).
[16] J. Dudek, B. Herskind, W. Nazarewicz, Z. Szymański and T. Werner, Phys. Rev. **C38**, 940 (1988).
[17] W. Nazarewicz, R. Wyss and A. Johnson, Phys. Lett. **225B**, 208 (1989).
[18] W. Nazarewicz, R. Wyss and A. Johnson, Nucl. Phys. **A503**, 285 (1989).
[19] W. Satuła, R. Wyss, and P. Magierski, Nucl. Phys. **A578**, 45 (1994).
[20] P. Fallon, A. Alderson, M.A. Bentley, A.M. Bruce, P.D. Forsyth, D. Howe, J.W. Roberts, J.F. Scharpey-Schafer, P.J. Twin, F.A. Beck, Th. Byrski, D. Curien and C. Schuck, Phys. Lett. **B218**, 137 (1989).
[21] Th. Byrski, F.A. Beck, D. Curien, C. Schuck, P. Fallon, A. Alderson, I .Ali, M.A. Bentley, A.M. Bruce, P.D. Forsyth, D. Howe, J.W .Roberts, J.F. Scharpey-Schafer, G. Smith and P.J. Twin, Phys. Rev. Lett. **64**, 1650 (1990).
[22] G. deFrance, B. Haas, I. Ragnarsson, P.J. Twin, C.W. Beausang, F.A. Beck, Th. Byrski, S. Clarck, P.J. Dagnall, D. Curien, G. Duchêne, P. Fallon, S. Flibotte, S. Frobes, P.D. Forsyth, B. Kharraja, J.C. Lisle, J.C. Merdinger, C.M. Petrache, D. Prévost, J.F. Scharpey-Schafer, J. Simpson, J.P. Vivien and K. Zuber, Phys. Lett. **B331**, 290 (1994).
[23] B. Kharraja, Th. Byrski, F.A. Beck, C.W. Beausang, M.A. Bentley, D. Curien, P.J. Dagnall, G. Duchêne, S. Flibotte, G. de France, Zs. Fulop, B. Haas, A.Z. Kiss, J.C. Lisle, C.M. Petrache, Ch. Theisen, P.J. Twin, J.P. Vivien and K. Zuber, Phys. Lett. **B341**, 268 (1995).
[24] C.W. Beausang, S.A. Forbes, P. Fallon, P.J. Twin, J.N. Mo, J.C. Lisle, M.A. Bentley, J. Simpson, F.A. Beck, D. Curien, G. deFrance, G. Duchêne and D. Popescu, Nucl. Instr. and Meth. **A313**, 37 (1992).
[25] F.A. Beck, Prog. Part. Nucl. Phys. **Vol 28**, 443 (1992).
[26] S. Ćwiok, J. Dudek, W. Nazarewicz, J. Skalski and T. Werner, Comput. Phys. Commun. **46**, 379 (1987).
[27] J. Dudek, Z. Szymanski, T. Werner, A. Faessler and C. Lima, Phys. Rev. **C26**, 1712 (1982).

[28] J. Dudek, W. Nazarewicz and P. Olanders, Nucl.Phys. **A420**, 285 (1984).
[29] B.K. Jennings and R.K.Bhaduri, Nucl.Phys. **A237**, 149 (1975).
[30] B.K. Jennings, R.K. Bhaduri and M. Brack, Nucl.Phys. **A253**, 29 (1978).
[31] V.M. Strutinsky, Nucl.Phys. **A95**, 420 (1967).
[32] V.M. Strutinsky, Nucl.Phys. **A122**, 1 (1968).
[33] M. Bolsterli, E.O. Fiset, J.R. Nix and J.L. Norton, Phys.Rev. **C5**, 1050 (1972).
[34] J. Dobaczewski and J. Dudek, Reports nucl-th/9611035 and nucl-th/9611036, submitted to Computer Physics Communications.
[35] D. Gogny, in Proc. Int. Conf. on Nuclear Physics, eds. J. De Boer and H. Mang (North-Holland, Amsterdam, 1973)
[36] D. Gogny, in Nuclear self-consistent fields, ed. G. Ripka and M. Porneuf (North-Holland, Amsterdam, 1975) p. 333
[37] J. Dechargé, M. Girod and D. Gogny, Phys. Lett. **55B**, 361 (1975).
[38] J. Dechargé and D. Gogny, Phys. Rev. C **21**, 1568 (1980).
[39] J.F. Berger, M. Girod and D. Gogny, Nucl. Phys. **A428**, 23c (1984).
[40] D. Vautherin and D.M. Brink, Phys. Rev. **C5**, 626 (1972).
[41] We use the quadrupole and hexadecapole moment operators normalized as $Q_{2\mu}=\sqrt{16\pi/5}r^2Y_{2\mu}$ ($Q_{20}=2z^2-x^2-y^2$), and $Q_{4\mu}=r^4Y_{4\mu}$
[42] For technical reasons explained in Ref. [34] we use the y axis as the cranking axis. In the present study we identify the projection of the angular momentum on the cranking axis with the total angular momentum.
[43] P. Ring and P. Schuck, The Nuclear Many-Body Problem (Springer, Berlin, 1980)
[44] H. Flocard, P. Quentin, A.K. Kerman, and D. Vautherin, Nucl. Phys. **A203**, 433 (1973).
[45] J. Bartel, P. Quentin, M. Brack, C. Guet, and H.B. Håkansson, Nucl. Phys. **A386**, 79 (1982).
[46] W. Nazarewicz, P.J. Twin, P. Fallon, and J.D. Garrett, Phys. Rev. Lett. **64**, 1654 (1990).
[47] I. Ragnarsson, Nucl. Phys. **A557**, 167c (1993).
[48] M. Beiner, H. Flocard, N. Van Giai and P. Quentin, Nucl. Phys. **A238**, 29 (1975).
[49] H. Savajols, A. Korichi, D. Ward, D. Appelbe, G.C. Ball, C. Beausang, F.A. Beck, T. Byrski, D. Curien, P. Dagnall, G. de-France, D. Disdier, G. Duchene, S. Erturk, C. Finck, S. Flibotte, B. Gall, A. Galindo-Uribarri, B. Haas, G. Hackman, V.P. Janzen, B. Kharraja, J.C. Lisle, J.C. Merdinger, S.M. Mullins, S. Pilotte, D. Prevost, D.C. Radford, V. Rauch, C. Rigollet, D. Smalley, M.B. Smith, O. Stezowski, J. Styczen, C. Theisen, P.J. Twin, J.P. Vivien, J.C. Waddington, K. Zuber, I. Ragnarsson, Phys. Rev. Lett. **76**, 4480 (1996).
[50] D. Nisius *et al.*, Abstracts, Int. Conf. on Nuclear Structure at the Limits, Argonne, 1996, Preprint ANL/PHY-96/1, p. 33.
[51] W. Satuła, J. Dobaczewski, J. Dudek, and W. Nazarewicz, Report nucl-th/9608019, Phys. Rev. Lett. **77** No. 26 (1996).
[52] S. Flibotte, H.R. Andrews, G.C. Ball, C.W. Beausang, F.A. Beck, G. Belier, T. Byrski, D. Curien, P.J. Dagnall, G. de France, D. Disdier, G. Duchêne, Ch. Finck, B. Haas, G. Hackman, D.S. Haslip, V.P. Janzen, B. Kharraja, J.C. Lisle, J.C. Merdinger, S.M. Mullins, W. Nazarewicz, D.C. Radford, V. Rauch, H. Savajols, J. Styczen, Ch. Theisen, P.J. Twin, J.P. Vivien, J.C. Waddington, D. Ward, K. Zuber, and S. Åberg, Phys. Rev.

Lett. **71**, 4299 (1993).
[53] I. Hamamoto and B. Mottelson, Phys. Lett. **B333**, 294 (1994).
[54] S. Frauendorf, J. Meng, and J. Reif, Proc. Int. Conf. on Physics from Large γ-ray Detector Arrays, Berkeley, 1994, Volume 2, LBL-35687, p. 52.
[55] P. Magierski, P.-H. Heenen, and W. Nazarewicz, Phys. Rev. **C51**, R2880 (1995).
[56] W.D. Luo, A. Bouguettoucha, J. Dobaczewski, J. Dudek, and X. Li, Phys. Rev. **C52**, 2989 (1995).
[57] F. Dönau, S. Frauendorf, and J. Meng, Phys. Lett. B **387**, 667 (1996).
[58] A. Bouguettoucha, J. Dobaczewski, J. Dudek, W.D. Luo, and H. Molique, to be submitted to Physical Review C.
[59] J. Dudek, A. Majhofer and J. Skalski, J. Phys. (London) **G6**, 447 (1980).
[60] W. Nazarewicz, J. Dudek, and Z. Szymanski, Nucl. Phys. **A436**, 139 (1985).

TABLES

TABLE I. Experimental γ-ray energies (in keV) in SD Bands 1 and 2 in ^{151}Tb.

Band 1	Band 2
.	646.5(2)
.	691.6(2)
.	737.0(2)
768.4(2)	782.5(2)
810.9(2)	828.6(2)
854.0(2)	874.5(2)
897.5(2)	921.4(2)
942.7(2)	*968.6(2)*
988.4(2)	1015.6(2)
1034.7(2)	1063.0(2)
1081.9(2)	1110.9(2)
1129.9(2)	1158.9(2)
1178.7(2)	1206.9(2)
1228.0(2)	1255.0(2)
1278.0(2)	1303.1(2)
1328.5(2)	1351.4(2)
1379.9(2)	1399.7(2)
1431.4(2)	1448.3(2)
1483.6(2)	*1496.5(6)*
1535.8(3)	1545.2(6)
1589.6(1.7)	.

TABLE II. Theoretical configurations of eight bands in ^{151}Tb and the values of exit spins predicted within the HF method with the SkM* force and no pairing. The exit-spin values correspond to states fed by the last measured γ transition identified in the last column. The value calculated for Band 1 equals to $I_o^{(1)}=69/2\hbar$. An estimated effect of pairing (see text) would bring this value down to $61/2\hbar$. Exit spins of all other bands are given with respect to $I_o^{(1)}$. When more than one configuration could be a candidate (e.g. in the case of Bands 5 to 7) at most two of them are presented in the Table. Spin differences are given in $\hbar$ and the transition energies in keV. The second column gives the total parities and signatures of the bands analyzed.

Band	$(\pi$,r)	Configuration	$I_o - I_o^{(1)}$	$E_\gamma^{I_o+2\to I_o}$
1	$(+,-i)$	$\nu(22,22,21,21),\pi(15,16,17,17)$	0	768.4
2	$(-,-i)$	$\pi[3,0,1]1/2(r{=}+i) \to \pi[6,6,0]1/2(r{=}+i)$	-6	646.5
3	$(+,+i)$	$\pi[6,5,1]3/2(r{=}-i) \to \pi[6,6,0]1/2(r{=}+i)$	-3	727.1
4	$(-,+i)$	$\pi[3,0,1]1/2(r{=}-i) \to \pi[6,6,0]1/2(r{=}+i)$	$+3$	865.8
5	$(+,-i)$	$\nu[7,6,1]3/2(r{=}-i) \to \nu[5,2,1]3/2(r{=}-i)$	-2	710.1
5	$(-,-i)$	$\nu[7,6,1]3/2(r{=}-i) \to \nu[4,0,2]5/2(r{=}-i)$	-2	710.1
6	$(+,+i)$	$\nu[7,6,1]3/2(r{=}-i) \to \nu[5,2,1]3/2(r{=}+i)$	$+3$	838.2
6	$(-,+i)$	$\nu[7,6,1]3/2(r{=}-i) \to \nu[4,0,2]5/2(r{=}+i)$	$+3$	838.2
7	$(-,+i)$	$\pi[6,5,1]3/2(r{=}-i) \to \pi[5,3,0]1/2(r{=}+i)$	$+1$	753.9
7	$(-,+i)$	$\nu[7,6,1]3/2(r{=}-i) \to \nu[4,0,2]5/2(r{=}+i)$	-1	753.9
8	$(-,-i)$	$\nu[7,6,1]3/2(r{=}-i) \to \nu[4,0,2]5/2(r{=}-i)$	0	785.0

FIGURES

FIG. 1. Single-particle Routhians calculated for the ^{151}Tb nucleus by using the HF cranking formalism with the SkM* interaction. The solutions correspond to the reference configuration defined in Eq. (5.2). There are four families of curves corresponding to different parity-signature combinations, namely, the positive-parity Routhians are denoted with the full (r=$-i$) and dash-dotted (r=$+i$) lines, and the negative-parity Routhians are denoted with the dotted (r=$+i$) and long-dashed (r=$-i$) lines. Recall that the positive (negative) signature r=$+i$ (r=$-i$) corresponds to the negative (positive) signature exponent $\alpha = -\frac{1}{2}$ ($\alpha = +\frac{1}{2}$), the latter notation used by some other authors. The curves are labeled using the standard Nilsson labels $[N, n_z, \Lambda]\Omega$ with the sign of the signature r added at the end. They correspond to dominant components of the calculated wave functions at ω= 0 (left set of labels) and ω= 0.8 (right set of labels).

FIG. 2. Similar to that in Fig. 1 but using the SIII parametrization of the Skyrme interactions. The reference configuration has been defined in Eq. (5.2).

FIG. 3. Single-particle Routhians analogous to those shown in Fig. 1 but for the WS cranking Hamiltonian. With increasing values of ω, the deformation parameters (β_2,γ,β_4) vary so as to minimize the total energy (calculated by making use of the Strutinsky method) of the reference configuration (5.2).

FIG. 4. Comparison of the calculated dynamical moments (in $\hbar^2$/MeV) for the yrast configuration in ^{151}Tb without (top, f=1) and with (bottom, f=0.9) the scaling procedure described in the text.

FIG. 5. Energy as a function of spin for the proton particle-hole configurations corresponding to the low-lying excitations in ^{151}Tb. To increase the legibility of the Figure some configurations are presented in the top part and other in the bottom part. The labels at the right-hand-side define the single-nucleonic particle-hole configurations: the first label gives the hole state, while the one following the symbol ($\rightarrow$) corresponds to the particle state. The reference configuration is given in Eq. (5.2). The labels on the left-hand-side give the total parity and the total signature of the given configuration. In addition, the configurations are numbered in an arbitrary way, and these numbers are used as subscripts to facilitate the identification of configurations. The lines used to denote different parity-signature combinations are identical to those used in Fig. 1. The scaling has been applied here to conform with the standard of presentation in Fig. 4.

FIG. 6. Same as in Fig. 5 for the low-lying neutron configurations.

FIG. 7. The dynamical moments (in $\hbar^2$/MeV) of the lowest-energy bands corresponding to proton excitations presented in Fig. 5. A presence of at least two types of behavior (two "families" of bands) deserves noticing; those presented in the bottom part differ systematically from those in the top part. To facilitate the comparison between the curves the vacuum (reference) band has been repeated in both, i.e., the top and the bottom parts.

FIG. 8. Similar to that in Fig. 7 but for the low-lying neutron configurations. Here at least three characteristic forms of behavior are present. The configurations placed in the bottom part of the Figure give the slopes which are systematically smaller than those in the top part. Among the latter ones the bands demonstrating the crossings in the vicinity of the $\hbar\omega \sim 0.7$ MeV are clearly visible.

FIG. 9. A comparison of dynamical moments (in $\hbar^2$/MeV) for selected bands presented in Figs. 7 and 8 with experimental data for Bands 2 (top), 3 (middle), and 4 (bottom).

FIG. 10. The dynamical moments (in $\hbar^2$/MeV) for the neutron configuration proposed for Bands 5 (top) and 6 (bottom), compared to the experimental data.

FIG. 11. Illustration of the possible proton and neutron configurations as those describing the structure of Bands 7 (top) and 8 (middle). The dynamical moments (in $\hbar^2$/MeV) are nearly indistinguishable in proton and neutron configurations, while the corresponding proton quadrupole moments (bottom) are markedly different.

FIG. 12. Evolution of the proton axial moments Q_{20} and Q_{40} as functions of the angular momentum. The configurations discussed in the text are shown. To gain space the bands are labeled by the $(\pi, r)_n$-symbols which coincide with those used in previous Figures and are also listed in Table II.

FIG. 13. Proton quadrupole moments as functions of the dynamical moments (in $\hbar^2$/MeV) for all eight bands corresponding to these observed experimentally. Note that the high values of the quadrupole moments correspond to the *low* spin limit (cf. also Fig. 12).

FIG. 14. Comparison with the experimental data of the calculated kinematical (bottom) and dynamical (top) moments (in $\hbar^2$/MeV) for the yrast configuration in ^{152}Dy. Here the cranking WS method was applied with deformations $\beta_2 = 0.61$ and $\beta_4 = 0.12$. A small variation of the deformation with increasing rotation was not taken into account here since we are interested in this case in the effect of the global mechanisms (geometrical scaling, pairing force coupling) similar at any deformation. Full lines represent the total quantities, i.e., sums of the proton and neutron contributions; labels "t/pair" ("t/no-p") correspond to the pairing correlations being included (neglected) respectively. Separate proton and neutron contributions with and without pairing are also shown. The scaling factor is f=0.9. The $\mathcal{J}^{(1)}$ moments are obtained from the experimental data by applying the calculated exit-spin value of I_o=24 for the state fed by the E_γ=602.4 keV transition.

FIG. 15. Similar as in Fig. 14, but for the yrast configuration in ^{150}Gd. Deformations used: $\beta_2 = 0.58$ and $\beta_4 = 0.09$. The $\mathcal{J}^{(1)}$ moments are obtained from the experimental data by applying the calculated exit-spin value of I_o=32 for the state fed by the E_γ=815 keV transition.

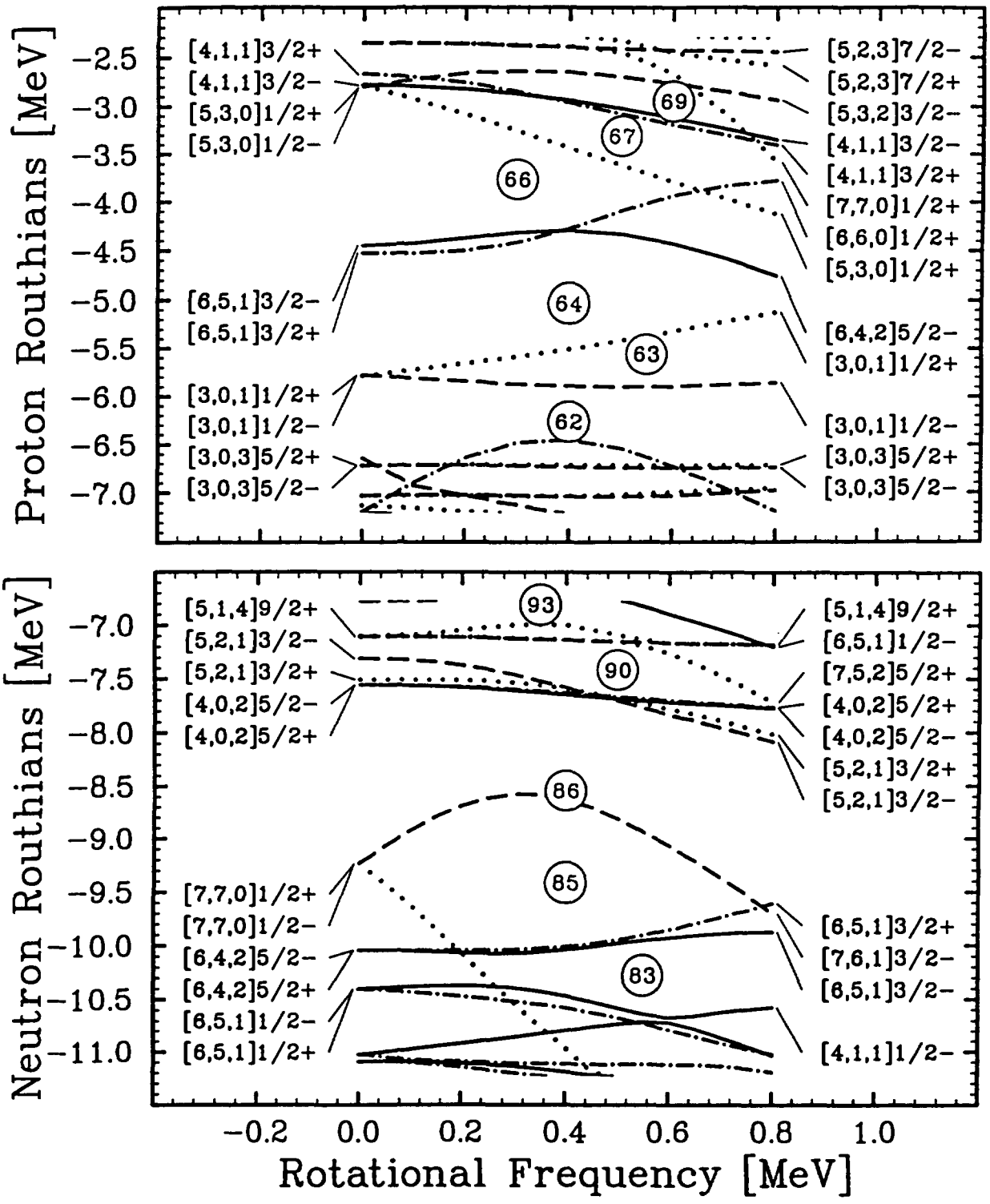
Proton Routhians [MeV]
−2.5
−3.0
−3.5
−4.0
−4.5
−5.0
−5.5
−6.0
−6.5
−7.0
[4,1,1]3/2+
[4,1,1]3/2−
[5,3,0]1/2+
[5,3,0]1/2−
[6,5,1]3/2−
[6,5,1]3/2+
[3,0,1]1/2+
[3,0,1]1/2−
[3,0,3]5/2+
[3,0,3]5/2−
[5,2,3]7/2−
[5,2,3]7/2+
[5,3,2]3/2−
[4,1,1]3/2−
[4,1,1]3/2+
[7,7,0]1/2+
[6,6,0]1/2+
[5,3,0]1/2+
[6,4,2]5/2−
[3,0,1]1/2+
[3,0,1]1/2−
[3,0,3]5/2+
[3,0,3]5/2−
69
67
66
64
63
62
Neutron Routhians [MeV]
−7.0
−7.5
−8.0
−8.5
−9.0
−9.5
−10.0
−10.5
−11.0
[5,1,4]9/2+
[5,2,1]3/2−
[5,2,1]3/2+
[4,0,2]5/2−
[4,0,2]5/2+
[7,7,0]1/2+
[7,7,0]1/2−
[6,4,2]5/2−
[6,4,2]5/2+
[6,5,1]1/2−
[6,5,1]1/2+
[5,1,4]9/2+
[6,5,1]1/2−
[7,5,2]5/2+
[4,0,2]5/2+
[4,0,2]5/2−
[5,2,1]3/2+
[5,2,1]3/2−
[6,5,1]3/2+
[7,6,1]3/2−
[6,5,1]3/2−
[4,1,1]1/2−
93
90
86
85
83
−0.2
0.0
0.2
0.4
0.6
0.8
1.0
Rotational Frequency [MeV]

Fig. 1

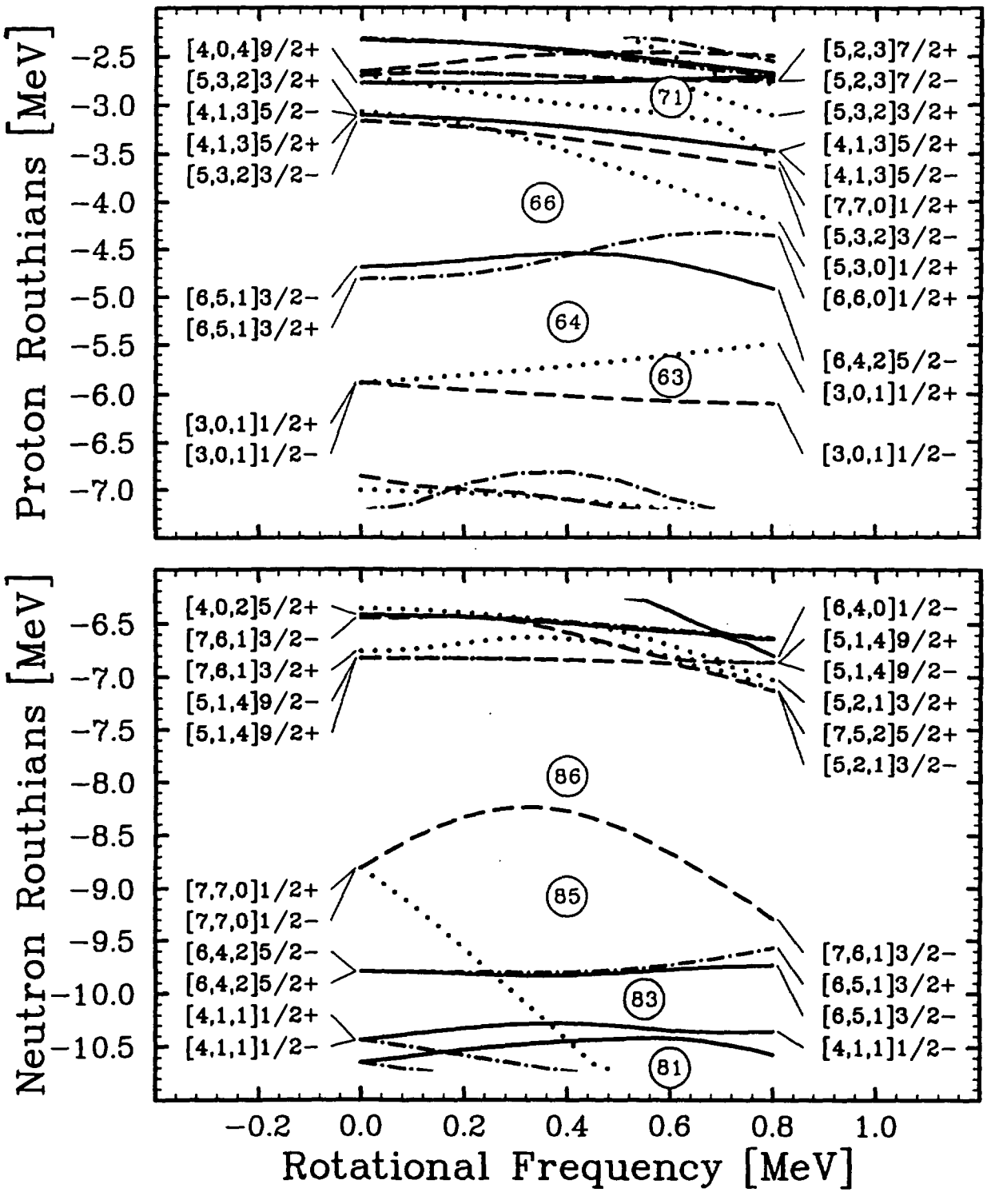
Proton Routhians [MeV]
−2.5
−3.0
−3.5
−4.0
−4.5
−5.0
−5.5
−6.0
−6.5
−7.0
[4,0,4]9/2+
[5,3,2]3/2+
[4,1,3]5/2−
[4,1,3]5/2+
[5,3,2]3/2−
[6,5,1]3/2−
[6,5,1]3/2+
[3,0,1]1/2+
[3,0,1]1/2−
71
66
64
63
[5,2,3]7/2+
[5,2,3]7/2−
[5,3,2]3/2+
[4,1,3]5/2+
[4,1,3]5/2−
[7,7,0]1/2+
[5,3,2]3/2−
[5,3,0]1/2+
[6,6,0]1/2+
[6,4,2]5/2−
[3,0,1]1/2+
[3,0,1]1/2−
Neutron Routhians [MeV]
−6.5
−7.0
−7.5
−8.0
−8.5
−9.0
−9.5
−10.0
−10.5
[4,0,2]5/2+
[7,6,1]3/2−
[7,6,1]3/2+
[5,1,4]9/2−
[5,1,4]9/2+
[7,7,0]1/2+
[7,7,0]1/2−
[6,4,2]5/2−
[6,4,2]5/2+
[4,1,1]1/2+
[4,1,1]1/2−
86
85
83
81
[6,4,0]1/2−
[5,1,4]9/2+
[5,1,4]9/2−
[5,2,1]3/2+
[7,5,2]5/2+
[5,2,1]3/2−
[7,6,1]3/2−
[6,5,1]3/2+
[6,5,1]3/2−
[4,1,1]1/2−
−0.2
0.0
0.2
0.4
0.6
0.8
1.0
Rotational Frequency [MeV]

Fig. 2

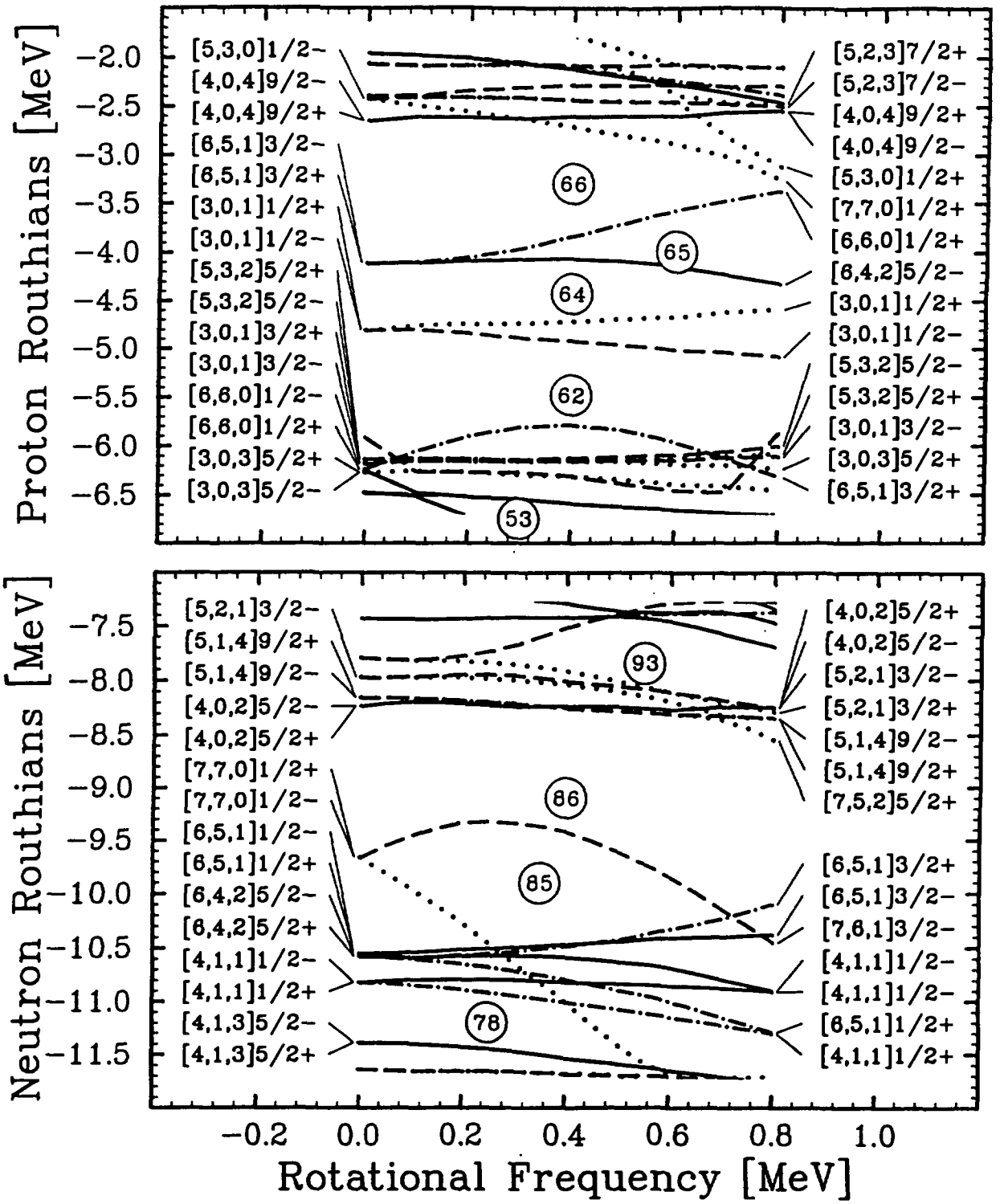
Proton Routhians [MeV]
−2.0
−2.5
−3.0
−3.5
−4.0
−4.5
−5.0
−5.5
−6.0
−6.5
[5,3,0]1/2−
[4,0,4]9/2−
[4,0,4]9/2+
[6,5,1]3/2−
[6,5,1]3/2+
[3,0,1]1/2+
[3,0,1]1/2−
[5,3,2]5/2+
[5,3,2]5/2−
[3,0,1]3/2+
[3,0,1]3/2−
[6,6,0]1/2−
[6,6,0]1/2+
[3,0,3]5/2+
[3,0,3]5/2−
66
65
64
62
53
[5,2,3]7/2+
[5,2,3]7/2−
[4,0,4]9/2+
[4,0,4]9/2−
[5,3,0]1/2+
[7,7,0]1/2+
[6,6,0]1/2+
[6,4,2]5/2−
[3,0,1]1/2+
[3,0,1]1/2−
[5,3,2]5/2−
[5,3,2]5/2+
[3,0,1]3/2−
[3,0,3]5/2+
[6,5,1]3/2+
Neutron Routhians [MeV]
−7.5
−8.0
−8.5
−9.0
−9.5
−10.0
−10.5
−11.0
−11.5
[5,2,1]3/2−
[5,1,4]9/2+
[5,1,4]9/2−
[4,0,2]5/2−
[4,0,2]5/2+
[7,7,0]1/2+
[7,7,0]1/2−
[6,5,1]1/2−
[6,5,1]1/2+
[6,4,2]5/2−
[6,4,2]5/2+
[4,1,1]1/2−
[4,1,1]1/2+
[4,1,3]5/2−
[4,1,3]5/2+
93
86
85
78
[4,0,2]5/2+
[4,0,2]5/2−
[5,2,1]3/2−
[5,2,1]3/2+
[5,1,4]9/2−
[5,1,4]9/2+
[7,5,2]5/2+
[6,5,1]3/2+
[6,5,1]3/2−
[7,6,1]3/2−
[4,1,1]1/2−
[4,1,1]1/2−
[6,5,1]1/2+
[4,1,1]1/2+
−0.2
0.0
0.2
0.4
0.6
0.8
1.0
Rotational Frequency [MeV]

Fig. 3

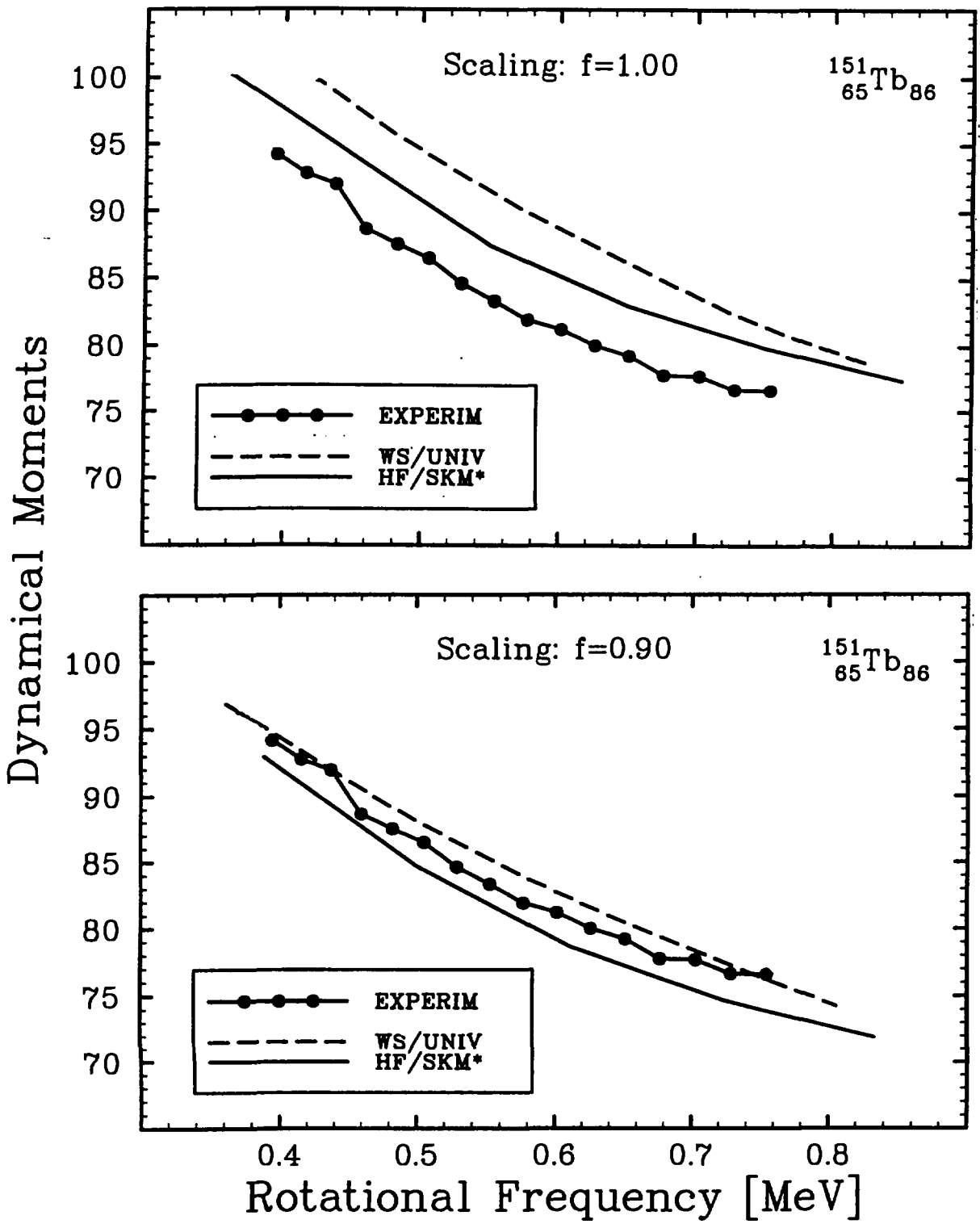
Scaling: f=1.00
$^{151}_{65}Tb_{86}$
EXPERIM
WS/UNIV
HF/SKM*
Scaling: f=0.90
$^{151}_{65}Tb_{86}$
EXPERIM
WS/UNIV
HF/SKM*
Dynamical Moments
100
95
90
85
80
75
70
0.4
0.5
0.6
0.7
0.8
Rotational Frequency [MeV]

Fig. 4

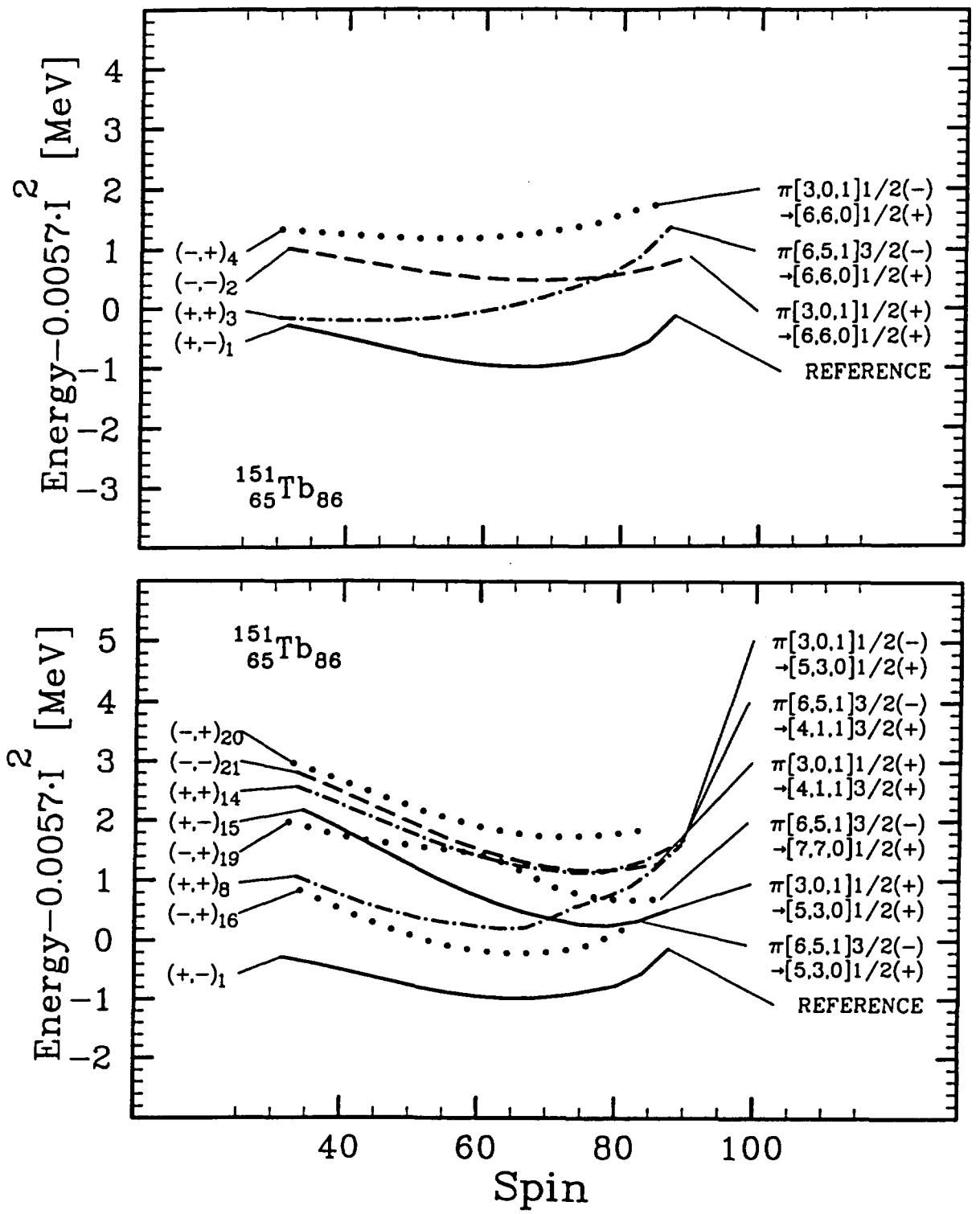
Energy−0.0057·I² [MeV]
(−,+)4
(−,−)2
(+,+)3
(+,−)1
π[3,0,1]1/2(−)
→[6,6,0]1/2(+)
π[6,5,1]3/2(−)
→[6,6,0]1/2(+)
π[3,0,1]1/2(+)
→[6,6,0]1/2(+)
REFERENCE
151 65Tb86
Energy−0.0057·I² [MeV]
151 65Tb86
(−,+)20
(−,−)21
(+,+)14
(+,−)15
(−,+)19
(+,+)8
(−,+)16
(+,−)1
π[3,0,1]1/2(−)
→[5,3,0]1/2(+)
π[6,5,1]3/2(−)
→[4,1,1]3/2(+)
π[3,0,1]1/2(+)
→[4,1,1]3/2(+)
π[6,5,1]3/2(−)
→[7,7,0]1/2(+)
π[3,0,1]1/2(+)
→[5,3,0]1/2(+)
π[6,5,1]3/2(−)
→[5,3,0]1/2(+)
REFERENCE
40
60
80
100
Spin

Fig. 5

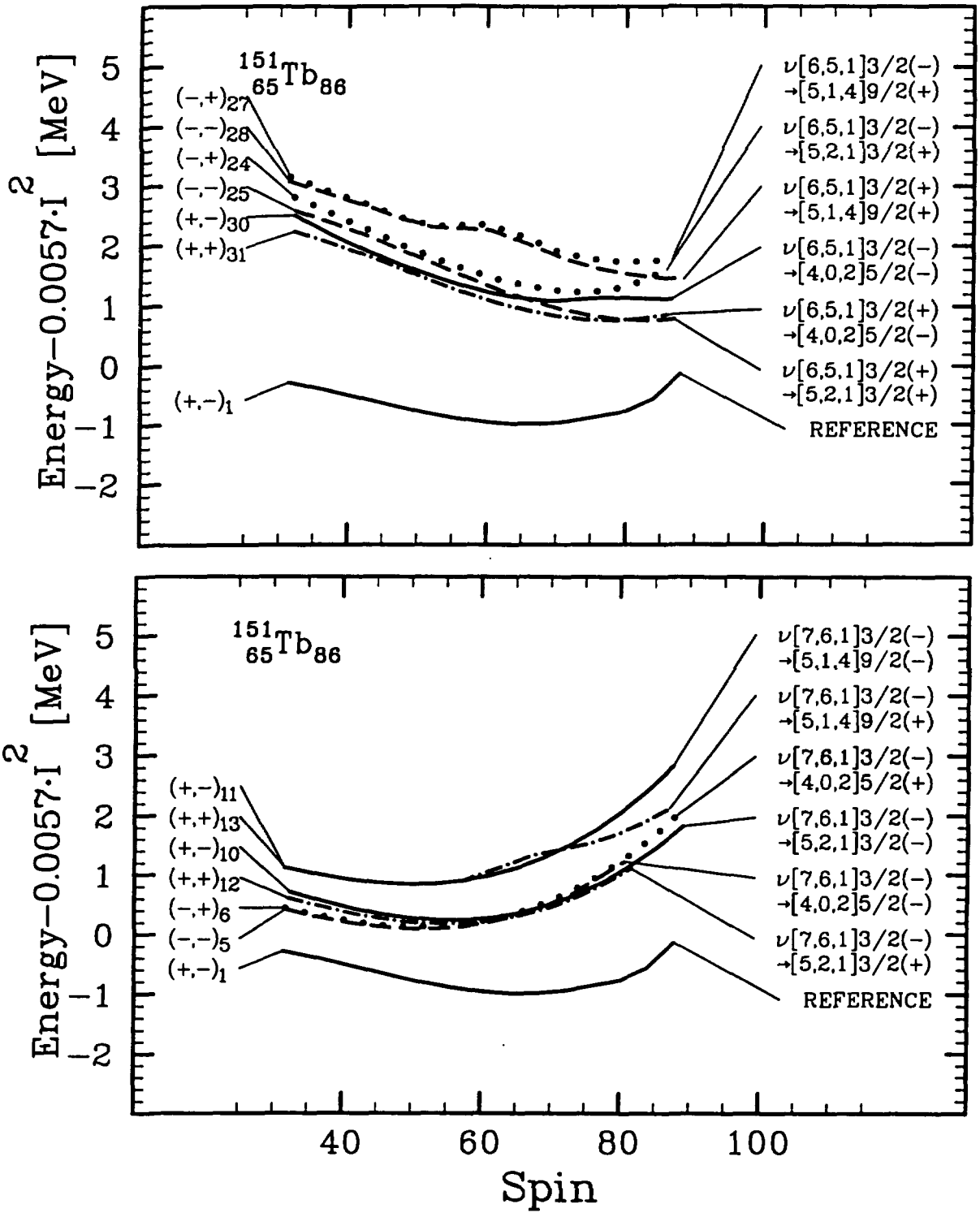
$^{151}_{65}Tb_{86}$
$(-,+)_{27}$
$(-,-)_{28}$
$(-,+)_{24}$
$(-,-)_{25}$
$(+,-)_{30}$
$(+,+)_{31}$
$(+,-)_1$
ν[6,5,1]3/2(−) →[5,1,4]9/2(+)
ν[6,5,1]3/2(−) →[5,2,1]3/2(+)
ν[6,5,1]3/2(+) →[5,1,4]9/2(+)
ν[6,5,1]3/2(−) →[4,0,2]5/2(−)
ν[6,5,1]3/2(+) →[4,0,2]5/2(−)
ν[6,5,1]3/2(+) →[5,2,1]3/2(+)
REFERENCE
$^{151}_{65}Tb_{86}$
$(+,-)_{11}$
$(+,+)_{13}$
$(+,-)_{10}$
$(+,+)_{12}$
$(-,+)_6$
$(-,-)_5$
$(+,-)_1$
ν[7,6,1]3/2(−) →[5,1,4]9/2(−)
ν[7,6,1]3/2(−) →[5,1,4]9/2(+)
ν[7,6,1]3/2(−) →[4,0,2]5/2(+)
ν[7,6,1]3/2(−) →[5,2,1]3/2(−)
ν[7,6,1]3/2(−) →[4,0,2]5/2(−)
ν[7,6,1]3/2(−) →[5,2,1]3/2(+)
REFERENCE
Energy−0.0057·I^2 [MeV]
5
4
3
2
1
0
−1
−2
40
60
80
100
Spin

Fig. 6

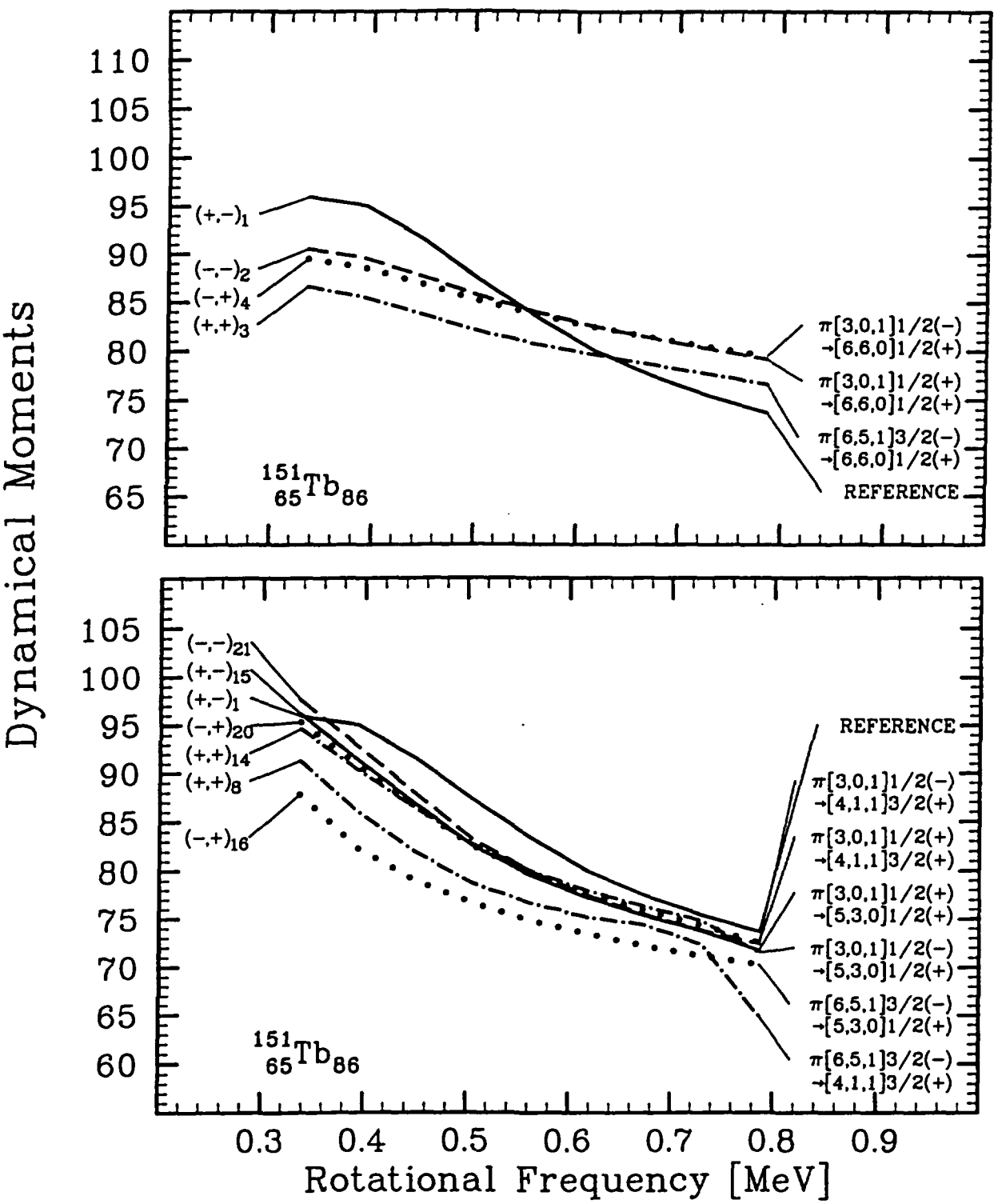
Dynamical Moments
110
105
100
95
90
85
80
75
70
65
$(+,-)_1$
$(-,-)_2$
$(-,+)_4$
$(+,+)_3$
$^{151}_{65}Tb_{86}$
$\pi[3,0,1]1/2(-)$
$\rightarrow[6,6,0]1/2(+)$
$\pi[3,0,1]1/2(+)$
$\rightarrow[6,6,0]1/2(+)$
$\pi[6,5,1]3/2(-)$
$\rightarrow[6,6,0]1/2(+)$
REFERENCE
105
100
95
90
85
80
75
70
65
60
$(-,-)_{21}$
$(+,-)_{15}$
$(+,-)_1$
$(-,+)_{20}$
$(+,+)_{14}$
$(+,+)_8$
$(-,+)_{16}$
$^{151}_{65}Tb_{86}$
REFERENCE
$\pi[3,0,1]1/2(-)$
$\rightarrow[4,1,1]3/2(+)$
$\pi[3,0,1]1/2(+)$
$\rightarrow[4,1,1]3/2(+)$
$\pi[3,0,1]1/2(+)$
$\rightarrow[5,3,0]1/2(+)$
$\pi[3,0,1]1/2(-)$
$\rightarrow[5,3,0]1/2(+)$
$\pi[6,5,1]3/2(-)$
$\rightarrow[5,3,0]1/2(+)$
$\pi[6,5,1]3/2(-)$
$\rightarrow[4,1,1]3/2(+)$
0.3
0.4
0.5
0.6
0.7
0.8
0.9
Rotational Frequency [MeV]

Fig. 7

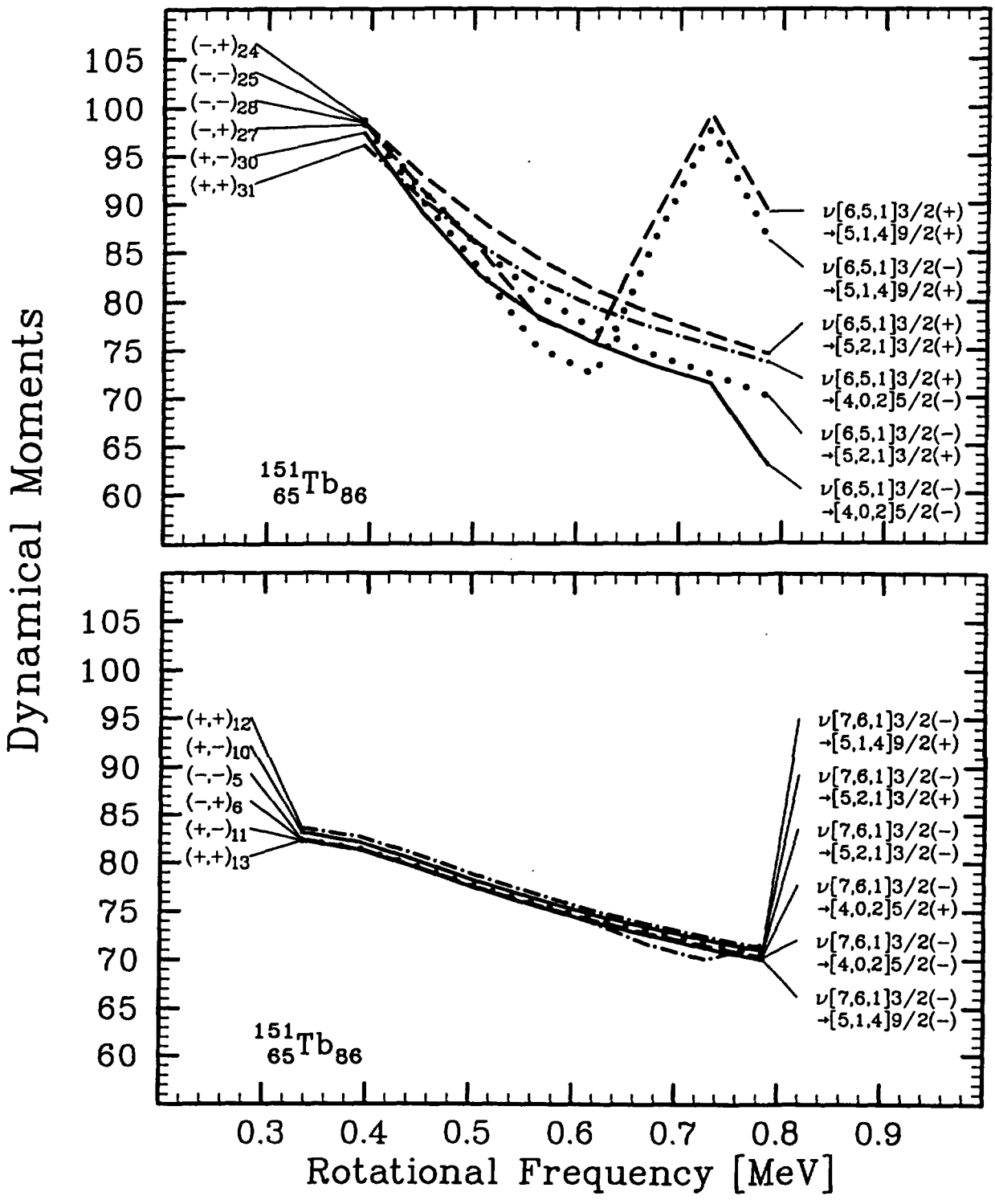
Dynamical Moments
105
100
95
90
85
80
75
70
65
60
(−,+)24
(−,−)25
(−,−)28
(−,+)27
(+,−)30
(+,+)31
ν[6,5,1]3/2(+)
→[5,1,4]9/2(+)
ν[6,5,1]3/2(−)
→[5,1,4]9/2(+)
ν[6,5,1]3/2(+)
→[5,2,1]3/2(+)
ν[6,5,1]3/2(+)
→[4,0,2]5/2(−)
ν[6,5,1]3/2(−)
→[5,2,1]3/2(+)
ν[6,5,1]3/2(−)
→[4,0,2]5/2(−)
151 65Tb86
(+,+)12
(+,−)10
(−,−)5
(−,+)6
(+,−)11
(+,+)13
ν[7,6,1]3/2(−)
→[5,1,4]9/2(+)
ν[7,6,1]3/2(−)
→[5,2,1]3/2(+)
ν[7,6,1]3/2(−)
→[5,2,1]3/2(−)
ν[7,6,1]3/2(−)
→[4,0,2]5/2(+)
ν[7,6,1]3/2(−)
→[4,0,2]5/2(−)
ν[7,6,1]3/2(−)
→[5,1,4]9/2(−)
151 65Tb86
0.3
0.4
0.5
0.6
0.7
0.8
0.9
Rotational Frequency [MeV]

Fig. 8

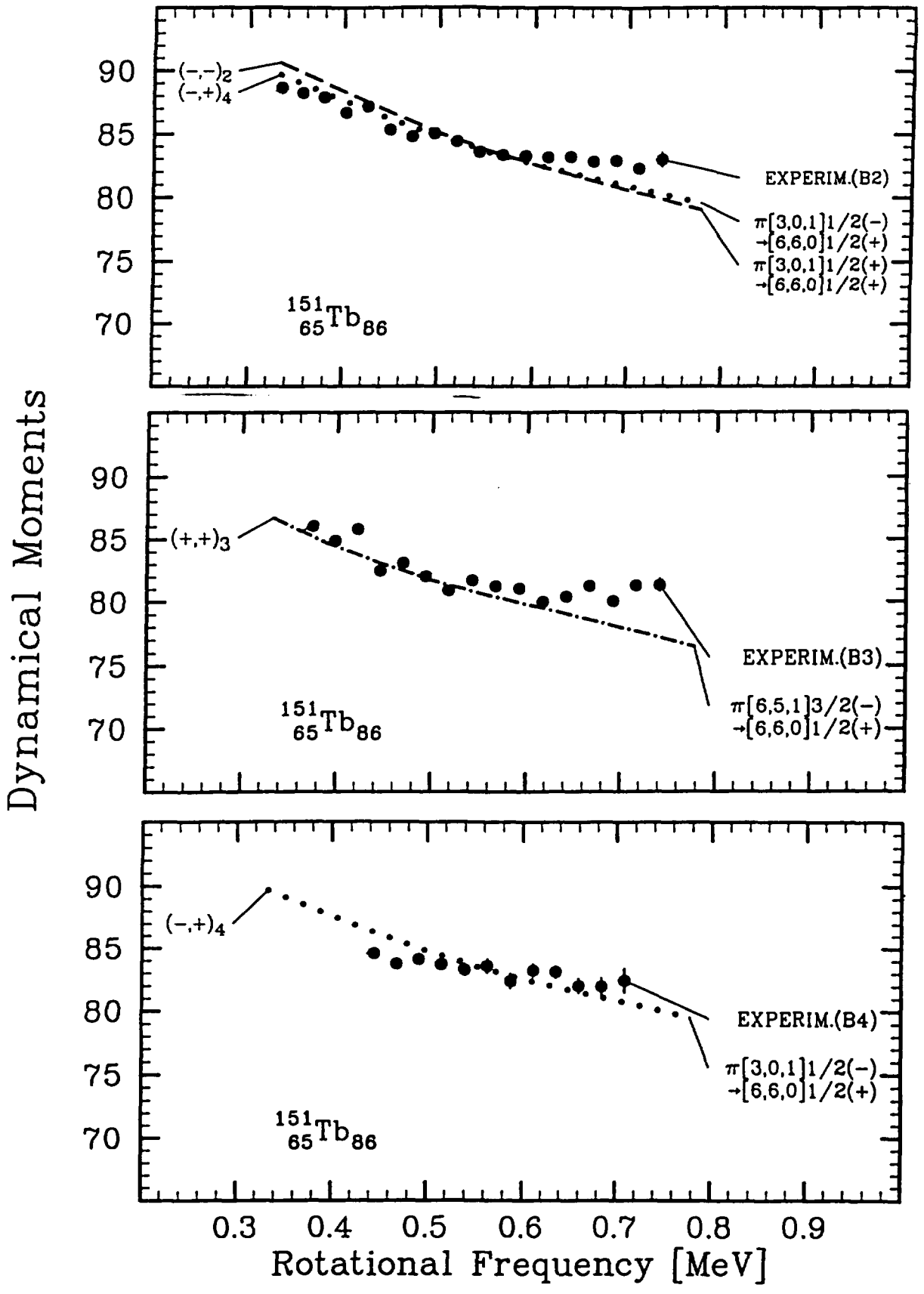
Dynamical Moments
90
85
80
75
70
$(-,-)_2$
$(-,+)_4$
EXPERIM.(B2)
π[3,0,1]1/2(-)
→[6,6,0]1/2(+)
π[3,0,1]1/2(+)
→[6,6,0]1/2(+)
$^{151}_{65}Tb_{86}$
$(+,+)_3$
EXPERIM.(B3)
π[6,5,1]3/2(-)
→[6,6,0]1/2(+)
$(-,+)_4$
EXPERIM.(B4)
π[3,0,1]1/2(-)
→[6,6,0]1/2(+)
0.3
0.4
0.5
0.6
0.7
0.8
0.9
Rotational Frequency [MeV]

Fig. 9

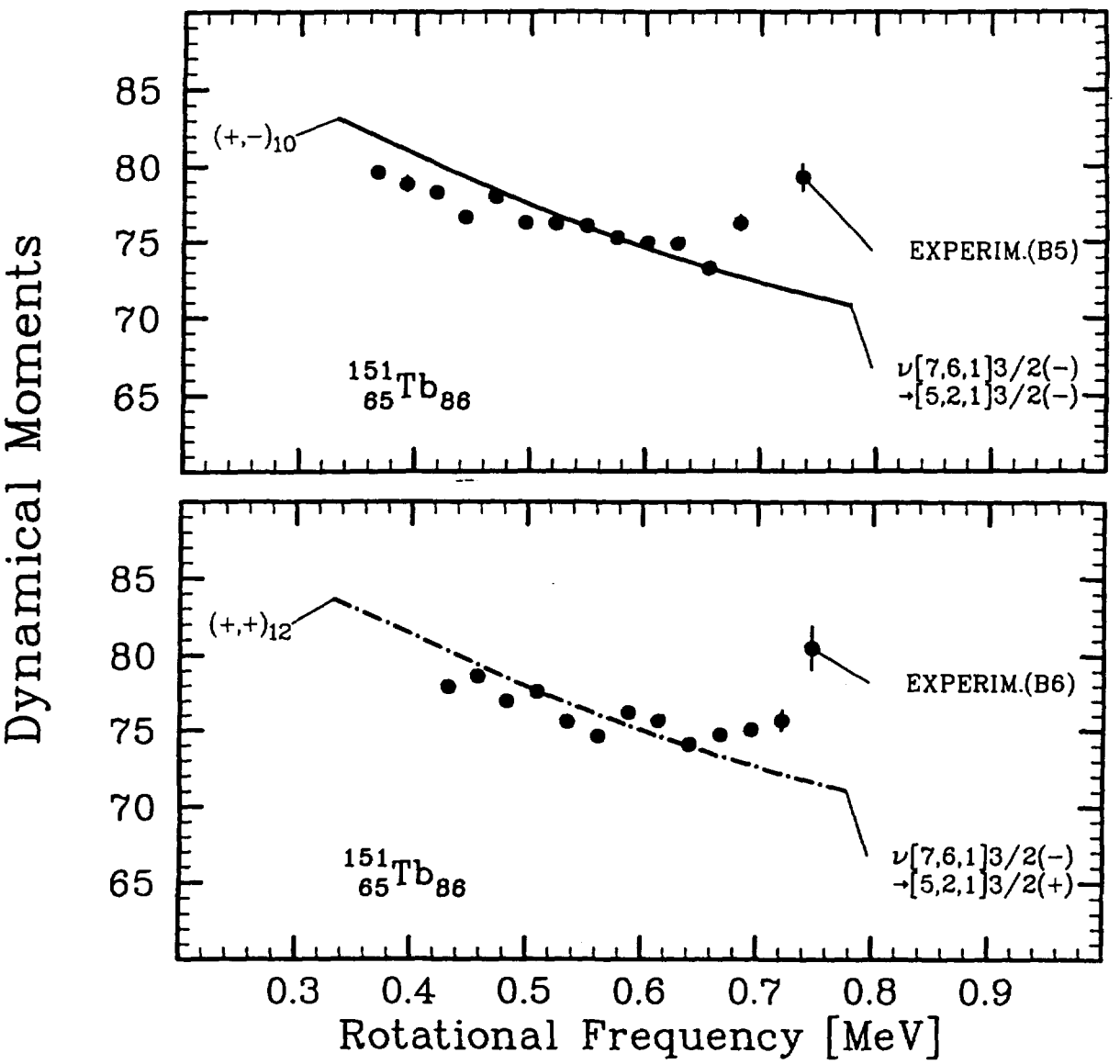
Dynamical Moments
85
80
75
70
65
(+,−)10
EXPERIM.(B5)
151 65Tb86
ν[7,6,1]3/2(−)
→[5,2,1]3/2(−)
85
80
75
70
65
(+,+)12
EXPERIM.(B6)
151 65Tb86
ν[7,6,1]3/2(−)
→[5,2,1]3/2(+)
0.3
0.4
0.5
0.6
0.7
0.8
0.9
Rotational Frequency [MeV]

Fig. 10

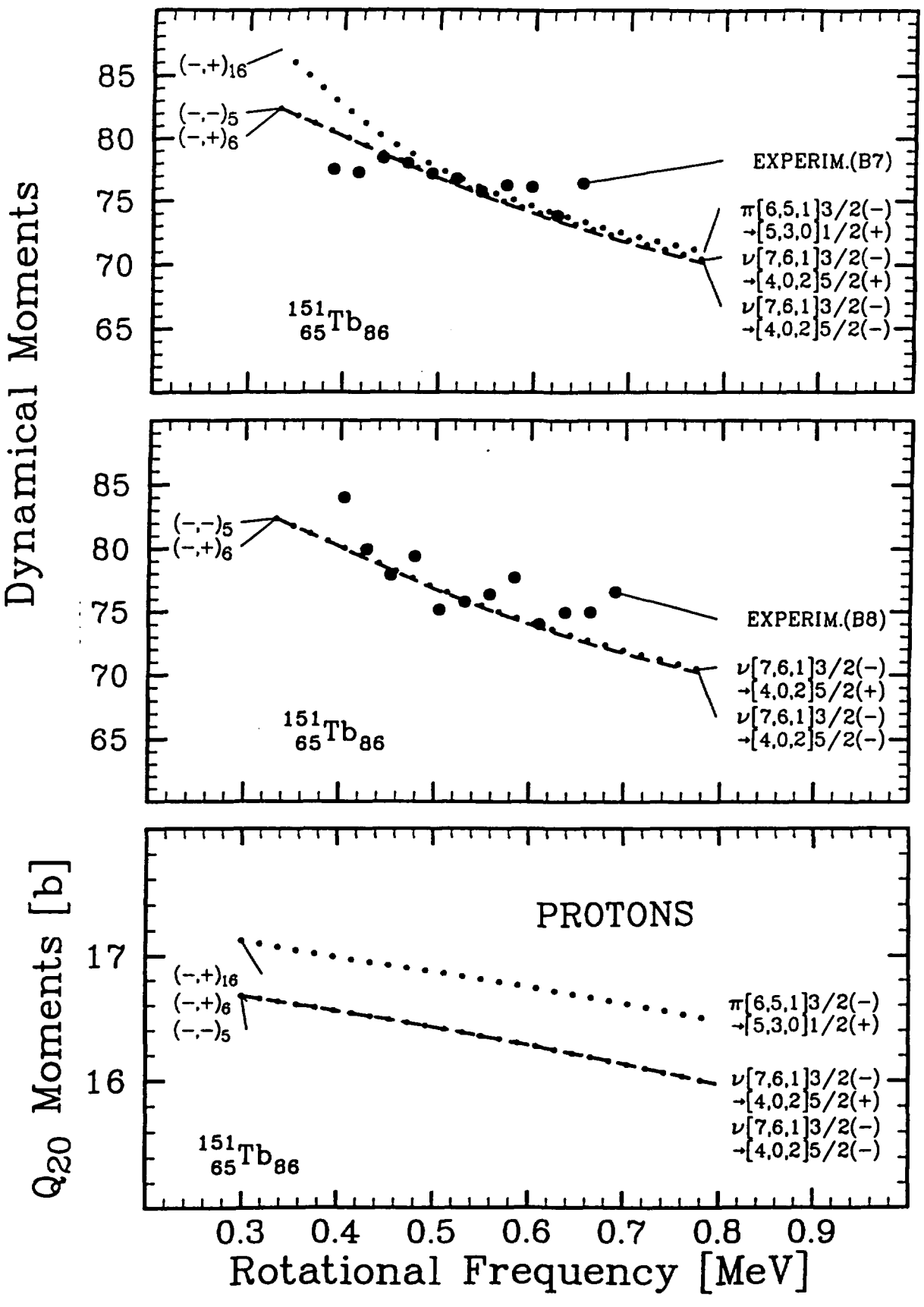
Dynamical Moments
85
80
75
70
65
(−,+)16
(−,−)5
(−,+)6
EXPERIM.(B7)
π[6,5,1]3/2(−)
→[5,3,0]1/2(+)
ν[7,6,1]3/2(−)
→[4,0,2]5/2(+)
ν[7,6,1]3/2(−)
→[4,0,2]5/2(−)
151 65Tb86
85
80
75
70
65
(−,−)5
(−,+)6
EXPERIM.(B8)
ν[7,6,1]3/2(−)
→[4,0,2]5/2(+)
ν[7,6,1]3/2(−)
→[4,0,2]5/2(−)
151 65Tb86
Q20 Moments [b]
PROTONS
17
16
(−,+)16
(−,+)6
(−,−)5
π[6,5,1]3/2(−)
→[5,3,0]1/2(+)
ν[7,6,1]3/2(−)
→[4,0,2]5/2(+)
ν[7,6,1]3/2(−)
→[4,0,2]5/2(−)
151 65Tb86
0.3
0.4
0.5
0.6
0.7
0.8
0.9
Rotational Frequency [MeV]

Fig. 11

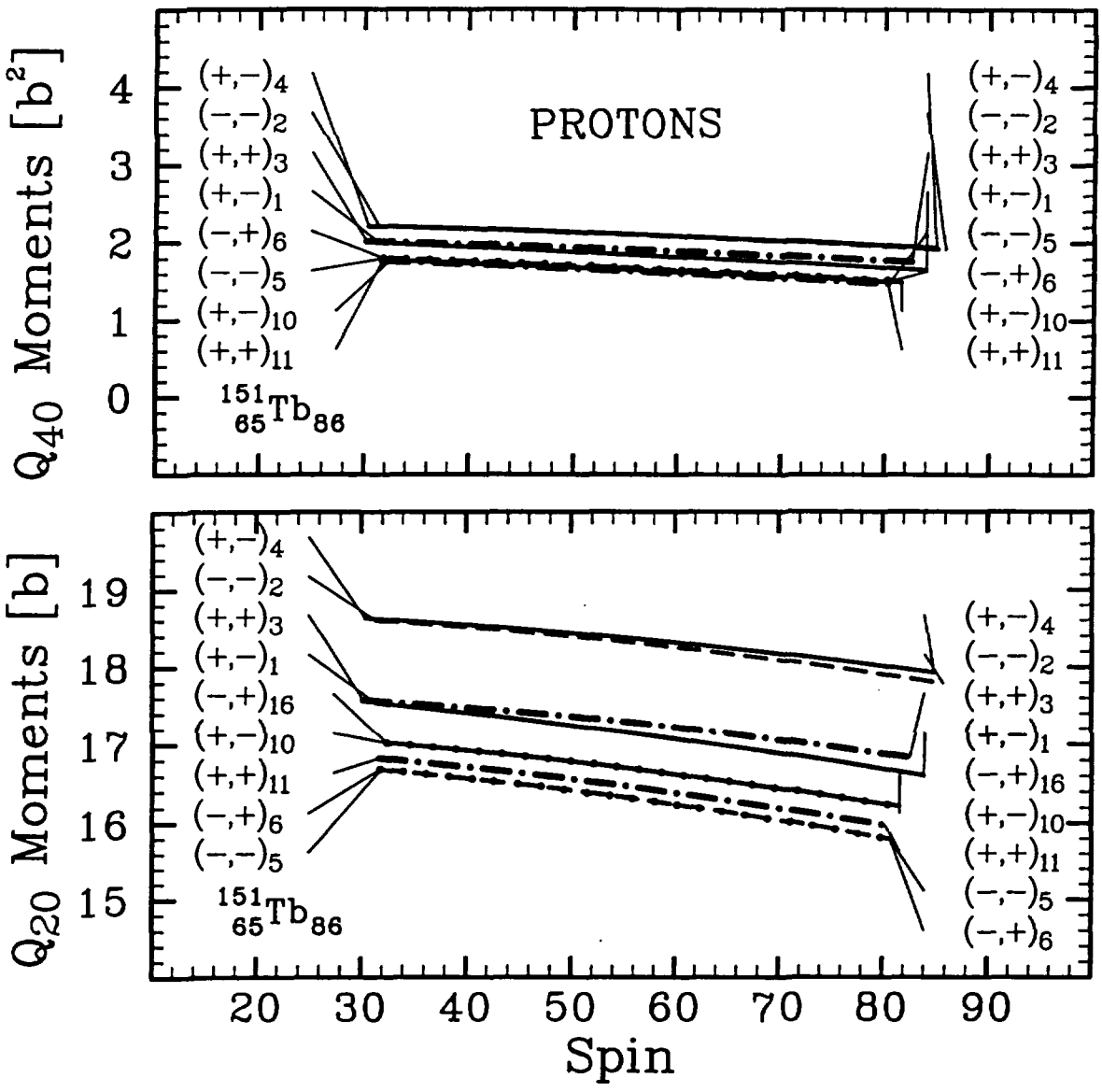
PROTONS
Q_{40} Moments [b^2]
Q_{20} Moments [b]
Spin
$^{151}_{65}Tb_{86}$
$(+,-)_4$
$(-,-)_2$
$(+,+)_3$
$(+,-)_1$
$(-,+)_6$
$(-,-)_5$
$(+,-)_{10}$
$(+,+)_{11}$
$(-,+)_{16}$

Fig. 12

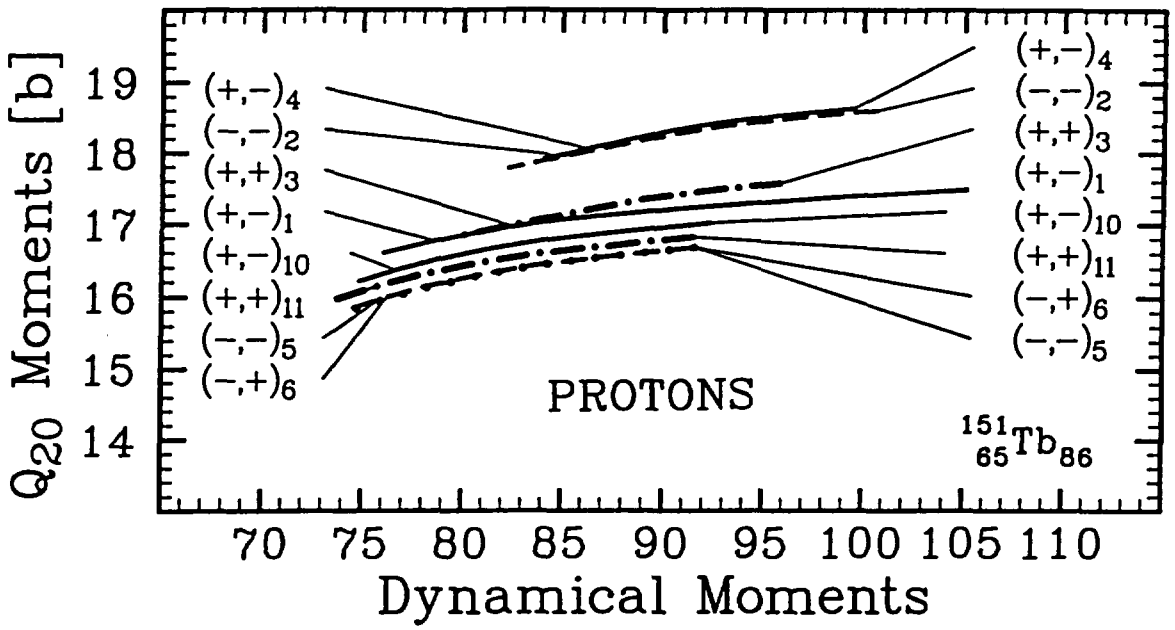
Q_{20} Moments [b]
19
18
17
16
15
14
$(+,-)_4$
$(-,-)_2$
$(+,+)_3$
$(+,-)_1$
$(+,-)_{10}$
$(+,+)_{11}$
$(-,-)_5$
$(-,+)_6$
PROTONS
$^{151}_{65}Tb_{86}$
70 75 80 85 90 95 100 105 110
Dynamical Moments

Fig. 13

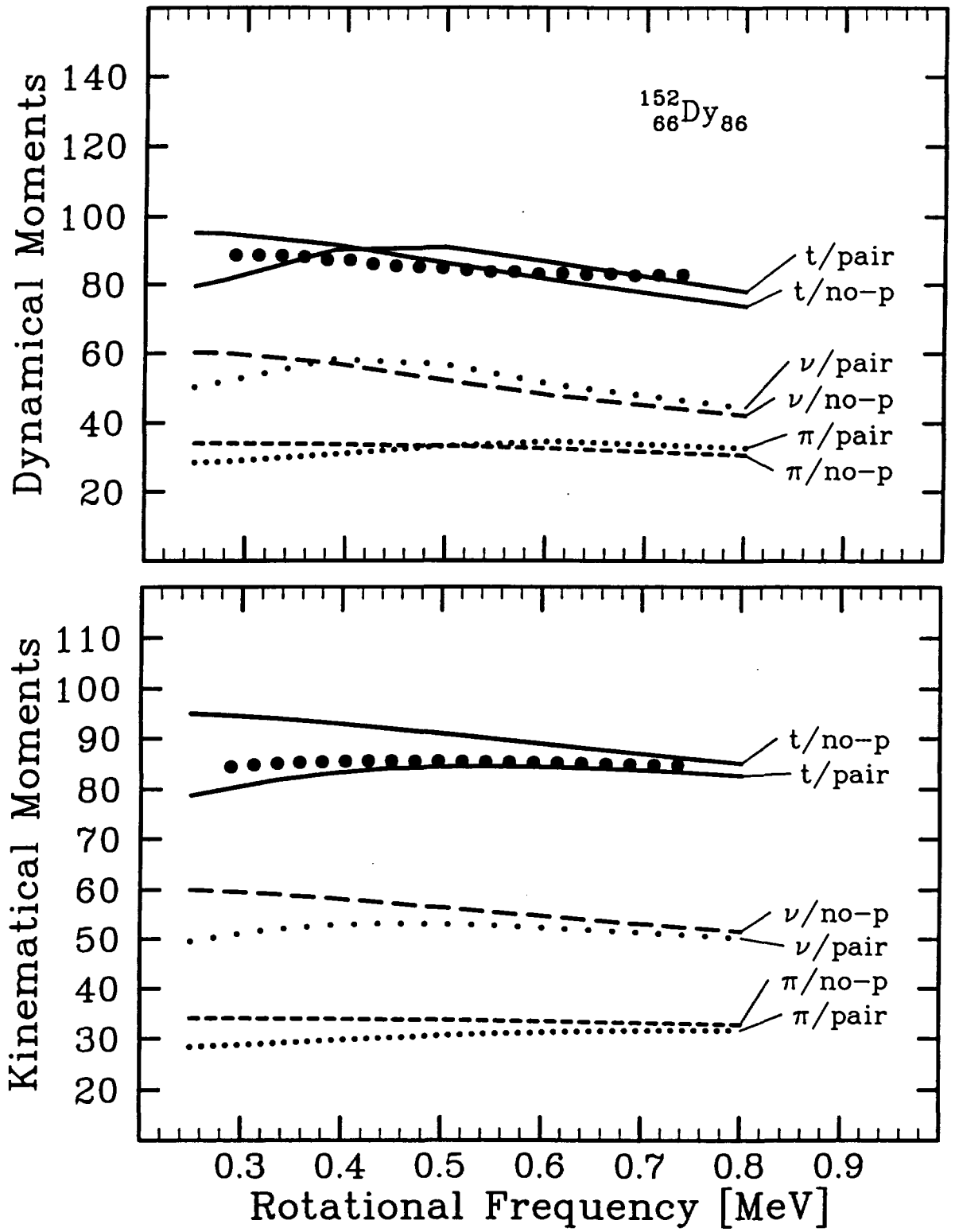
$^{152}_{66}Dy_{86}$
Dynamical Moments
140
120
100
80
60
40
20
t/pair
t/no-p
ν/pair
ν/no-p
π/pair
π/no-p
Kinematical Moments
110
100
90
80
70
60
50
40
30
20
t/no-p
t/pair
ν/no-p
ν/pair
π/no-p
π/pair
0.3
0.4
0.5
0.6
0.7
0.8
0.9
Rotational Frequency [MeV]

Fig. 14

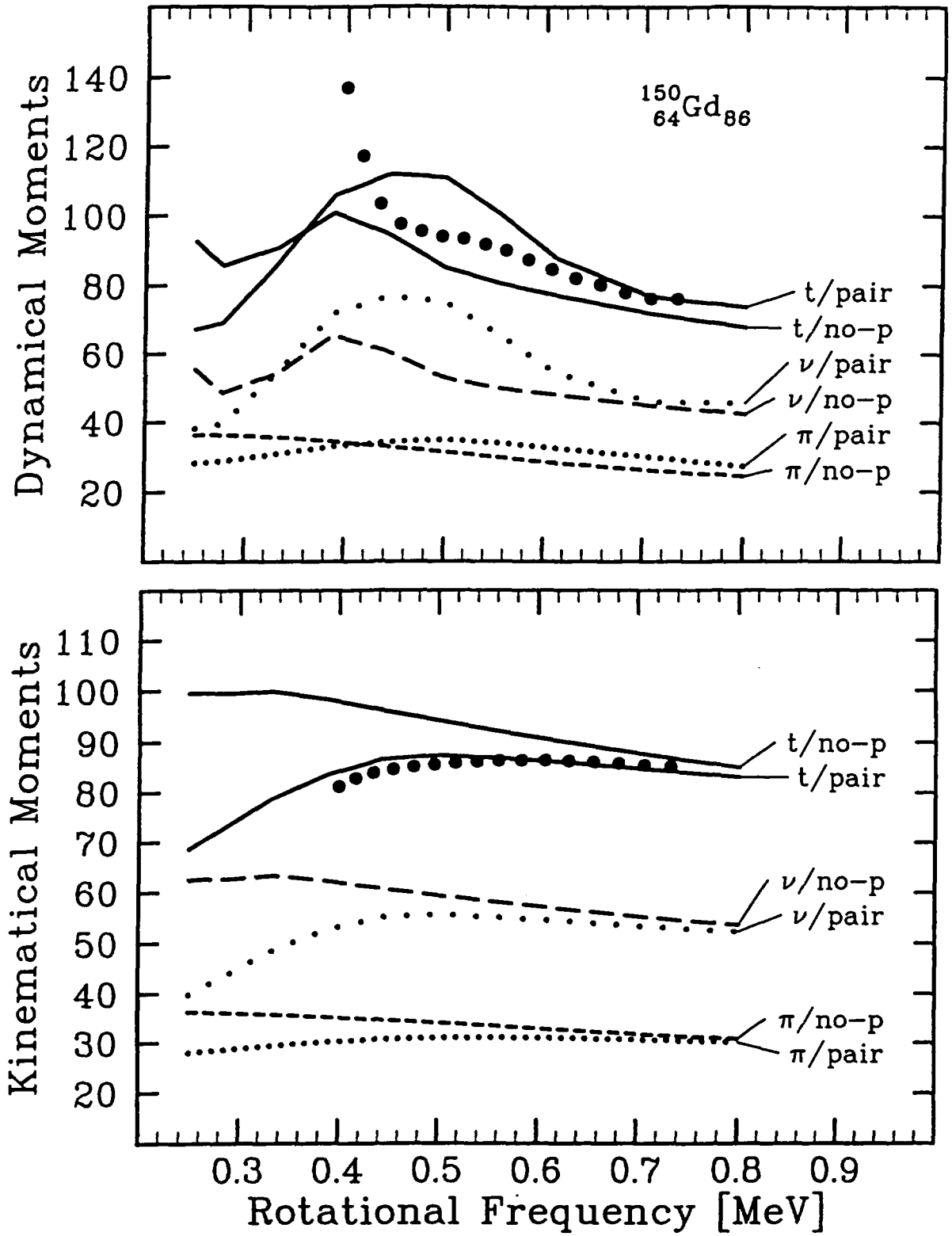
Dynamical Moments
140
120
100
80
60
40
20
$^{150}_{64}Gd_{86}$
t/pair
t/no-p
ν/pair
ν/no-p
π/pair
π/no-p
Kinematical Moments
110
100
90
80
70
60
50
40
30
20
t/no-p
t/pair
ν/no-p
ν/pair
π/no-p
π/pair
0.3
0.4
0.5
0.6
0.7
0.8
0.9
Rotational Frequency [MeV]

Fig. 15